Journal of Pathology
J Pathol 2009; **219**: 123–130
Published online 11 May 2009 in Wiley InterScience
(www.interscience.wiley.com) **DOI:** 10.1002/path.2576

Original Paper

Development of oligomeric prion-protein aggregates in a mouse model of prion disease

Kensuke Sasaki,* Haruhiko Minaki and Toru Iwaki
Department of Neuropathology, Neurological Institute, Graduate School of Medical Sciences, Kyushu University, Fukuoka, Japan

**Correspondence to:*
Kensuke Sasaki, Department of Neuropathology, Neurological Institute, Graduate School of Medical Sciences, Kyushu University, Fukuoka 812-8582, Japan.
E-mail: ksasaki@np.med.kyushu-u.ac.jp

No conflicts of interest were declared.

Received: 13 February 2009
Revised: 31 March 2009
Accepted: 5 May 2009

Abstract

In prion diseases the normal cellular isoform of prion protein (PrP), denoted PrP^{C}, is converted into an abnormal, pathogenic isoform of PrP (PrP^{Sc}). Diagnostic tools for prion diseases are conventionally based on the detection of protease-resistant PrP (PrP^{res}) after proteinase K digestion. However, recent studies have revealed that protease-sensitive abnormal PrP ($sPrP^{Sc}$) also exists in significant amounts in brains suffering from prion diseases. Here, we designed a simplified size-exclusion gel chromatography assay, using disposable spin columns to examine PrP aggregates in the course of the disease, without proteinase K digestion. Brain homogenates of NZW mice, inoculated intracranially with Fukuoka-1 strain, and which died at around 120 days post-inoculation, were assayed by this gel-fractionation method and eluted PrP molecules in each fraction were detected by western blot analysis. Oligomeric PrP molecules were well separated from monomers, as predicted. A conventional protease-digestion assay was also performed to detect PrP^{res} and revealed that the ratio of PrP^{res} to total PrP increased drastically from 105 days. However, the increase of PrP oligomers became significant from 90 days. These PrP oligomers in the early disease stage would, therefore, be $sPrP^{Sc}$ molecules that might affect the disease pathology, such as spongiform change and abnormal PrP deposition. We also observed that the resistance of PrP oligomers to proteinase K and insolubility in phosphotungstic acid precipitation increased with disease progression, which suggests that PrP oligomers are not clearly distinguished from cellular PrP or PrP^{res} but may overlap in a continuous spectrum. Our study casts light on the ambiguity of the definition of PrP^{Sc} and indicates that the abnormality of PrP molecules should be determined from various perspectives, more than protease resistance.

Keywords: prion; oligomer; transimissible spongiform encephalopathy; Creutzfeldt–Jakob disease; mouse model

Introduction

Transmissible spongiform encephalopathies (TSEs), also termed prion diseases, are fatal neurodegenerative diseases associated with abnormal deposition of prion protein (PrP) in the central nervous system. The normal cellular isoform of PrP, denoted PrP^{C}, is converted into an abnormal, protease-resistant, pathogenic isoform of PrP (PrP^{Sc}) by post-translational modification. The conversion of PrP^{C} into PrP^{Sc} involves a conformational change of the protein, from an α-helical to a β-sheet structure, and PrP^{Sc} forms detergent-insoluble aggregates and is partially resistant to proteinase K (PK) digestion [1]. Conventional diagnostic tools for prion diseases are based on the detection of protease-resistant abnormal PrP (PrP^{res} or $rPrP^{Sc}$) after PK digestion. However, recent studies have revealed that protease-sensitive abnormal PrP ($sPrP^{Sc}$) also exists at significant levels in TSE brains [2–5]. Due to the avoidance of protease digestion, conformation-dependant immunoassay (CDI) has been recently developed to detect total PrP^{Sc}, including $sPrP^{Sc}$ [3–7]. Other novel methods for the detection of PrP^{Sc} that do not require protease treatment have also been developed, such as sucrose gradient sedimentation and size-exclusion gel chromatography to detect abnormally aggregated PrP [8,9], fluorescence-based conformational biosensor to detect β-folded conformation of PrP [10], fluorescence correlation spectroscopy to detect prion particles [11] or modified sandwich ELISA to detect PrP oligomers [12].

It is well established that in many neurodegenerative diseases, designated as 'conformational diseases', the oligomeric form of disease-causing protein is more lethally neurotoxic than the highly aggregated fibrillar form. Amyloid β protein in Alzheimer's disease [13,14], α-synuclein in Lewy body disease [15] and polyglutamine protein in polyglutamine diseases

[16] form pathogenic oligomers that give rise to channel-forming structures, which lead to inappropriate membrane permeabilization [17,18]. In this context, protein aggregation into amyloid fibrils might be a protective process for the nervous system [19]. PrP^{Sc} also aggregates into oligomers or fibrils, whose minimal structures have recently been modelled as β-helical PrP trimers [20,21] reminiscent of channel-forming structures. Thus, toxic PrP peptide could form ion-permeable channels in lipid bilayer membranes [22]. Indeed, recent studies have indicated that PrP oligomers have more intense infectivity [23] and neurotoxicity [24,25] than highly aggregated amyloid fibrils, which corresponds to soluble amyloid β oligomers in Alzheimer's disease [13,14].

To explore the PrP molecules with intermediate properties between PrP^{C} and PrP^{res}, such as $sPrP^{Sc}$ or PrP oligomers, we developed a simplified size-exclusion gel chromatography assay using disposable gel-filtration spin columns. This method provides a tool for measuring the aggregation status of total PrP without PK digestion and to detect PrP oligomers in an easy and safe way. We employed this method to examine the time course for the development of PrP aggregates in a TSE mouse model. We also determined the characteristics of detected PrP oligomers to evaluate their association with disease progression.

Materials and methods

TSE mouse model

NZW mice were inoculated intracranially with the mouse-adopted Fukuoka-1 strain derived from a human case with Gerstmann–Sträussler–Scheinker disease [26]. Brain samples were serially collected twice a month until the mice died at around 120 days post-inoculation. At each time point, three brains were fixed in 10% formalin for pathological examination and three to four brains were frozen together in a single test tube for biochemical analyses. Control samples were also collected from the mock-treated mice, which had been inoculated with normal brain homogenate. Formalin-fixed, paraffin-embedded sections were stained with haematoxylin and eosin (H&E) to examine spongiform change, neuronal loss and gliosis. Spongiform change was assessed by image-analysis software (ImageJ, National Institutes of Health, USA), in which the highlighted area of vacuoles was calculated and divided by the total area, designated as a spongiform index [vacuolar/total area (%)]. Data were compared between groups at each time point using Tukey's test. Immunohistochemistry for PrP was performed using a polyclonal anti PrP C-terminal antibody (1 : 200; IBL, Japan) in conjunction with the detergent autoclaving method for antigen retrieval [27]. The procedures performed in this study were approved by the Committee of Ethics on Animal Experiments of the Faculty of Medicine, Kyushu University, and were in strict accordance with the Guidelines for Animal Experiments of the Faculty of Medicine, Kyushu University, and with Law No. 105 and Notification No. 6 of the Japanese Government.

Detection of PrP^{res}

Conventional procedures for the detection of PrP^{res} were conducted as follows: 1% brain homogenate was prepared in extraction buffer (100 mM Tris–HCl, 100 mM NaCl, 10 mM EDTA, 0.5% Nonidet P-40, 0.5% sodium deoxycholate, pH 7.6) and incubated with 50 μg/ml PK at 37 °C for 1 h. Protease activity was then abolished by the addition of 1 mM Pefabloc SC (Roche, USA). Undigested PrP^{res} fragments were separated by SDS–polyacrylamide gel electrophoresis (SDS–PAGE) in 12% NuPAGE Bis–Tris gels (Invitrogen, USA) and transferred onto polyvinilidene difluoride membranes (Millipore, USA). Protein was detected using anti-PrP mAb (clone SAF-83, raised against scrapie-associated fibrils from infected hamster brain, 1 : 10 000; Cayman, USA) as the primary antibody and peroxidase-labelled donkey anti-mouse IgG Ab (AP192P, 1 : 20 000; Chemicon, USA) as the secondary antibody, and visualized by chemiluminescence with ECL-plus substrate (GE Healthcare, UK). Another anti-PrP SAF-70 mAb (Cayman) recognizing amino acid residues 142–160 was also used to determine the specificity.

Spin-column gel filtration

We tested the spin-column kit CHROMA SPIN-200 (Clontech, USA) for its ability to fractionate proteins according to molecular size. The manufacturer's instructions refer to the size-selective separation and purification of nucleic acids, which indicate the capability to retrieve nucleic acids of >350 bases and eliminate proteins <1000 kDa; thus, we had to modify the procedures to enable the fractionation of proteins. Briefly, low-speed centrifugation following additional loads of extraction buffer were repeated to collect size-selected fractions. The modified protocol is summarized in Figure 1A. Columns were pre-spun at 200 × *g* for 3 min to remove storage buffer. Buffer exchange was made by the addition of 500 μl extraction buffer followed by centrifugation at 200 × *g* for 3 min. This step was then repeated. For easier sample loading, 0.01% bromophenol blue was added to 1% brain homogenates and then 75 μl sample was applied on the gel bed. Elution fractions were gathered into collection tubes by spinning at 120 × *g* for 2 min. Fractions were serially collected by repeated addition of 40 μl extraction buffer followed by centrifugation. Fractionated PrP was detected without PK treatment by SDS–PAGE and western blot analysis, as described above.

To evaluate fractionation profiles produced by this method, we applied western protein standards, MagicMark XP (Invitrogen, USA), to a spin column. Marker

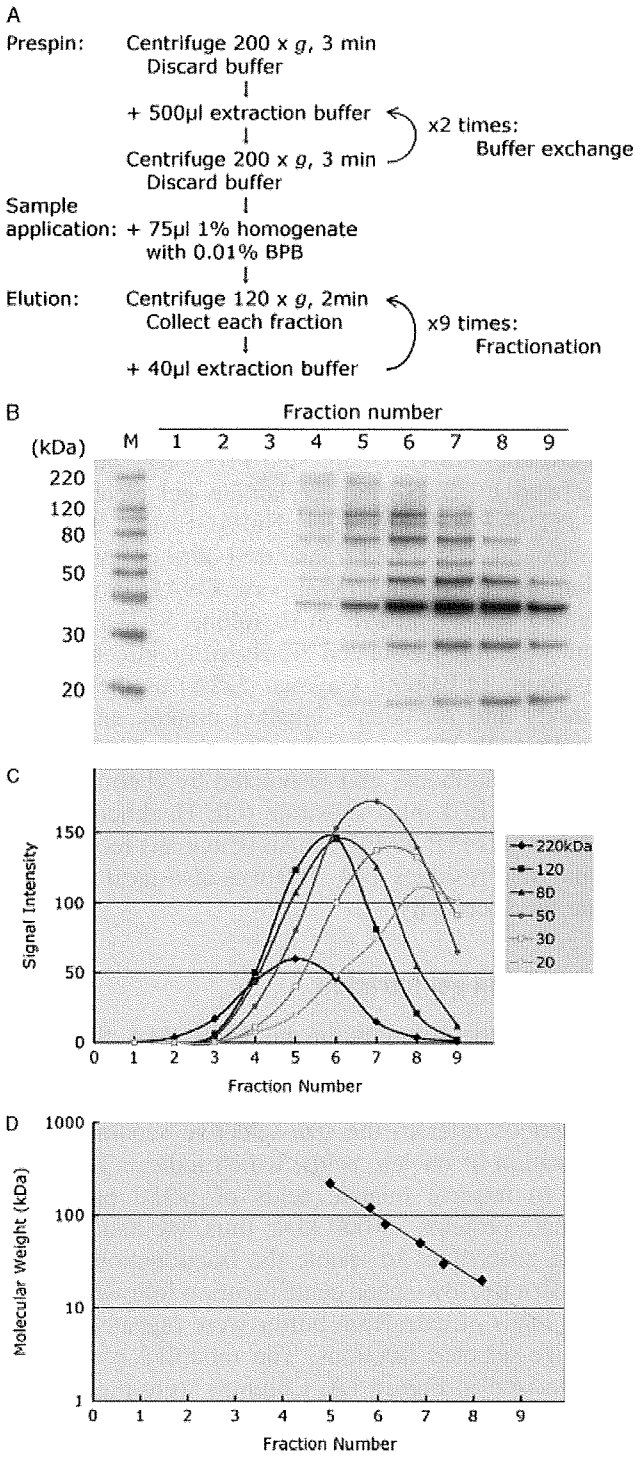

Figure 1. The fractionation capability of spin columns. (A) Protocol for the spin-column gel filtration method. CHROMA SPIN TE-200 (Clontech) columns were used. BPB, bromophenol blue. (B–D) Molecular-weight markers [MagicMark XP, Invitrogen; lane M in (B)] were gel-fractionated. The marker molecules eluted in each fraction were evaluated by SDS–PAGE (B) and a chromatogram was obtained from grey value measurements (C). Peak fractions of each molecule were estimated and plotted against molecular weight (kDa) (D). A log-linear relation was observed among 20–220 kDa molecules

proteins were prepared in sample buffer (NuPAGE LDS sample buffer; Invitrogen), to mimic the molecular size in the condition of SDS–PAGE, and fractionated by the spin-column gel filtration method. Each fraction was assessed by western blot analysis, as described above.

Biochemistry of fractionated PrP

PrP molecules in each fraction prepared by the gel-filtration method were examined for protease resistance using 50 µg/ml PK treatment to detect PrP^{res}, as described above. Phosphotungstic acid (PTA) precipitation was also conducted on each fraction, without PK treatment, to estimate the total disease-associated PrP^{Sc}, as described previously [28] except avoiding the enrichment effect. Specifically, 10 µl fractions were treated with PTA and the resulting pellets were resuspended in 10 µl sample-loading buffer. Prepared PrP molecules were detected by western blot analysis, as described above. Deglycosylation by PNGase F (peptide-N-glycosidase F; New England Biolabs, USA) was also performed in accordance with the manufacturer's instructions to determine the PrP fragments unambiguously.

To determine whether fractionated PrP molecules have the form of oligomers, dot-blot analysis was performed using 2 µl each fraction dotted onto a nitrocellulose membrane. Oligomers were detected using a primary anti-oligomer antibody [29] (rabbit polyclonal A11, 1 : 5000, Invitrogen, USA) and peroxidase-labelled donkey anti-rabbit IgG Ab (AP187P, 1 : 10 000, Chemicon, USA) as the secondary antibody. The oligomer-specific immunoreaction was detected by a chemiluminescent assay.

Results

Fractionation capability of spin columns

The fractionation pattern of molecular weight markers, as shown in Figure 1B–D, indicated that the elution curve of each marker protein was rather broad, due to the low resolution of the column; however, the fractionation pattern appeared to be sufficiently effective to distinguish, by size, abnormally aggregated PrP oligomers from monomer PrP^{C}. Although fraction 1 consisted mostly of the void volume and contained insufficient protein to be assessed, the size of eluted protein molecules in fractions 2 and 3 was estimated to be >200 kDa in reference to the chromatogram and the standard curve of peak fractions (Figure 1C, D). Proteins whose molecular weights were approximately 30 kDa, such as monomer PrP molecules, were collected mainly in fractions 6–8.

Profiles of the NZW/Fukuoka-1 mouse model

NZW mice, inoculated intracranially with Fukuoka-1 strain, died approximately 120 days post-inoculation. Spongiform change in the thalamus was specifically prominent from 90 days (Figure 2A–C), while fine vacuolation and gliotic change in the cerebral cortex

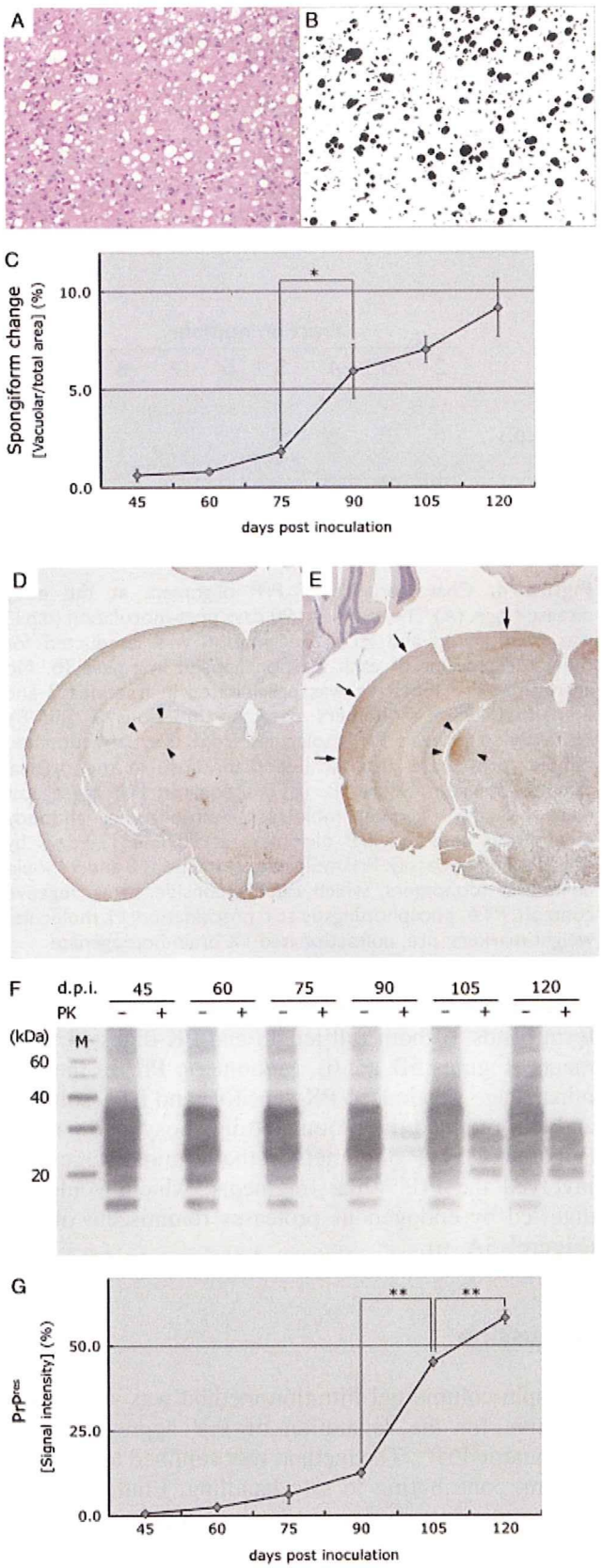

was observed from 105 days (data not shown). Abnormal PrP deposition, predominantly observed in a punctate synaptic pattern, was first detected by immunohistochemistry from 60 days in the lateral thalamic nucleus (Figure 2D, arrow heads), which became more intense with time (Figure 2E, arrow heads) and spread into the cerebral cortex from 105 days (Figure 2E, arrows). Even though PrP^{res} was already detected in 90 day samples, the ratio of PrP^{res} to total PrP increased significantly from 105 days (Figure 2F, G), which corresponded to the time course of abnormal PrP deposition spreading throughout the brain, including to the cerebral cortex.

Time course of the development of PrP aggregates

The spin-column gel filtration method revealed that PrP aggregates increased with respect to disease progression, and that the development of PrP oligomers preceded the appearance of PrP^{res}. Most of the PrP molecules extracted from the control and 45 day samples were monomers that were collected mainly in fractions 6–8 (Figure 3A, B). Meanwhile, PrP aggregates collected in fractions 2–4 were significantly increased from 90 days (Figure 3B, and the time-course chart shown in Figure 3C), which preceded the augmentation of PrP^{res} from 105 days. In the early disease stage, fractionated PrP aggregates at 90 days were not effectively retrieved by PTA precipitation (Figure 4A), although these molecules were certainly in the form of oligomers, as indicated by the dot-blot analysis with anti-oligomer antibody (Figure 4B). In the terminal disease stage, fractionated PrP oligomers at 120 days acquired an unexpectedly high level of PK resistance (Figure 5B) and were precipitated in conjunction with PTA, even though the retrieved PrP molecules were apparently less than those in original fractions (Figure 5C).

Time course of the modification of PrP fragments

PNGase deglycosylation elucidated that total PrP consisted of full-length molecules and smaller fragments other than PrP^{res} (Figure 6), possibly derived from endogenous proteolytic cleavage [30], which caused complicated band patterns in western blot analyses. Anti-PrP SAF-70 mAb, which recognizes amino acid residues 142–160, also detected a similar fragment

Figure 2. Profiles of the NZW/Fukuoka-1 mouse model. (A–C) Assessment of the spongiform change in the lateral thalamic region. Coarse or fine vacuoles were specifically observed at 120 days post-inoculation. (A; H&E, magnification ×200). The area of vacuoles was highlighted (B) and calculated as the spongiform index [vacuolar/total area (%)] at each time point (C). Spongiform change in the thalamus was significantly exacerbated from 90 days ($^{*}p = 0.0011$, Tukey's test; three mice were examined at each point). (D, E) Time course of PrP deposition (immunohistochemistry for PrP, magnification ×12.5). Representative sections prepared at 60 (D) and 105 days (E) are shown. Punctate synaptic deposition of PrP was observed in the thalamus (arrowheads) and the cerebral cortex (arrows). (F, G) Development of PrP^{res}. The signal intensity index was calculated as the percentage of the density of PK-resistant PrP against total PrP without PK treatment (G). The ratio of PrP^{res} was drastically increased from 105 days ($^{**}p < 0.0001$, Tukey's test; experiments were performed in triplicate). PK, proteinase-K treatment; M, molecular weight markers

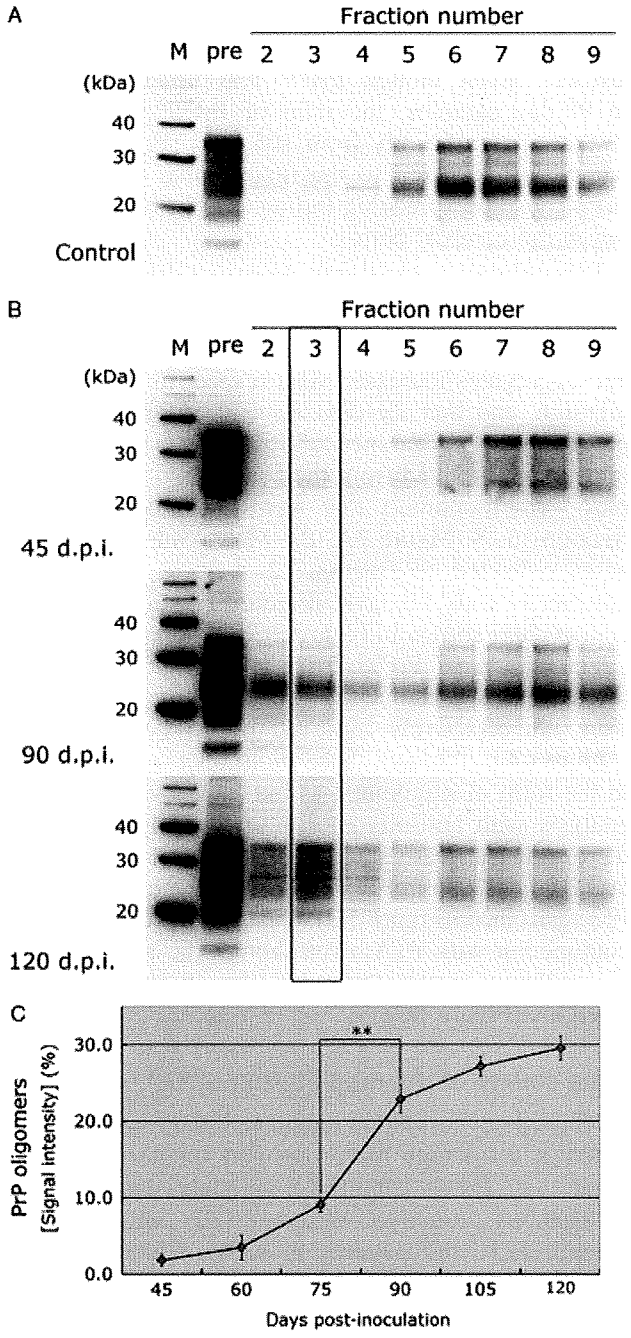

Figure 3. The development of PrP aggregates precedes the appearance of PrP^{res} molecules. (A, B) The PrP molecules in 1% brain homogenates were fractionated by spin-columns and detected by western blot analysis. Representative results of the control sample collected at 120 days post mock-inoculation (A), and the diseased samples at 45, 90 and 120 days post-inoculation (d.p.i.) (B) are shown. (C) The signal intensity index of PrP oligomers [fraction 3 in (B)] was calculated as the percentage against total PrP [pre in (B)]. PrP aggregates were significantly increased from 90 days (**$p < 0.0001$, Tukey's test; experiments were performed in triplicate). M, molecular weight markers; pre, unfractionated 1% brain homogenates were loaded to provide the index of total PrP

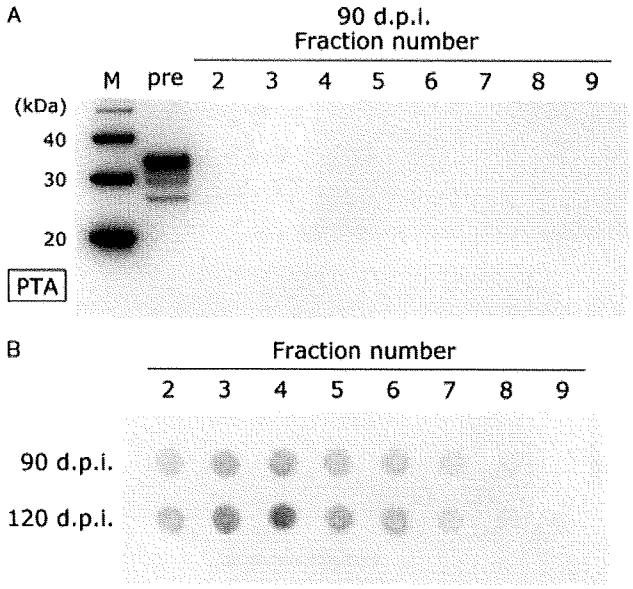

Figure 4. Characteristics of PrP oligomers at the early disease stage. (A) The sample at 90 days post-inoculation (d.p.i.) was fractionated and PTA precipitation was conducted for the same amount of each fraction applied in Figure 3B. No aggregated PrP molecule was precipitated in fractions 2 and 3, neither were monomers detected (fractions 7 and 8). Note that retrieved PrP molecules from the unfractionated sample (pre) were also far less than those in the original sample shown in Figure 3B. (B) Fractionated PrP aggregates were certainly oligomer molecules. Anti-oligomer antibody (Invitrogen) detected PrP oligomers at 90 and 120 days by dot-blot immunoassay. PrP molecules in fractions 8 and 9 should be mostly monomers, which can be considered as negative controls. PTA, phosphotungstic acid precipitation; M, molecular weight markers; pre, unfractionated 1% brain homogenate

pattern (data not shown). PK-sensitive PrP in the control and also PrP oligomers in the early disease stage showed a prominent diglycosylated form, of both full-length and endogenously truncated fragments (Figures 3A, B, 6), whereas PrP^{res} in the terminal stage showed almost even quantities of three glycoform bands, of both full-length and PK-digested fragments (Figures 5B, C, 6). Monomeric PrP in the terminal stage was indeed PK-sensitive and PTA-soluble, and still retained the prominent diglycosylated pattern (Figure 5A). PrP oligomers in the terminal stage also involved the PrP^{res}-like fragments, which would be digested by endogenous proteases reminiscent of PK (Figures 5A, 6).

Discussion

The spin-column gel filtration method was simple yet effective for the separation of PrP aggregates and monomeric PrP^{C}. The method was confined to a closed system, contributing to safe handling. Elution curves were rather broad, due to the low resolution of the column; however, monomer PrP molecules, retrieved mainly in fractions 6–8, were well demarcated from oligomers in fractions 2–4, in accordance with our expectations. The reproducibility of the technique was confirmed, as shown in Figure 3B, in which standard deviations of the data at each time point were sufficiently small to compare each group statistically. The peak fraction of oligomers detected by dot-blot was found in fraction 4, which was slightly later

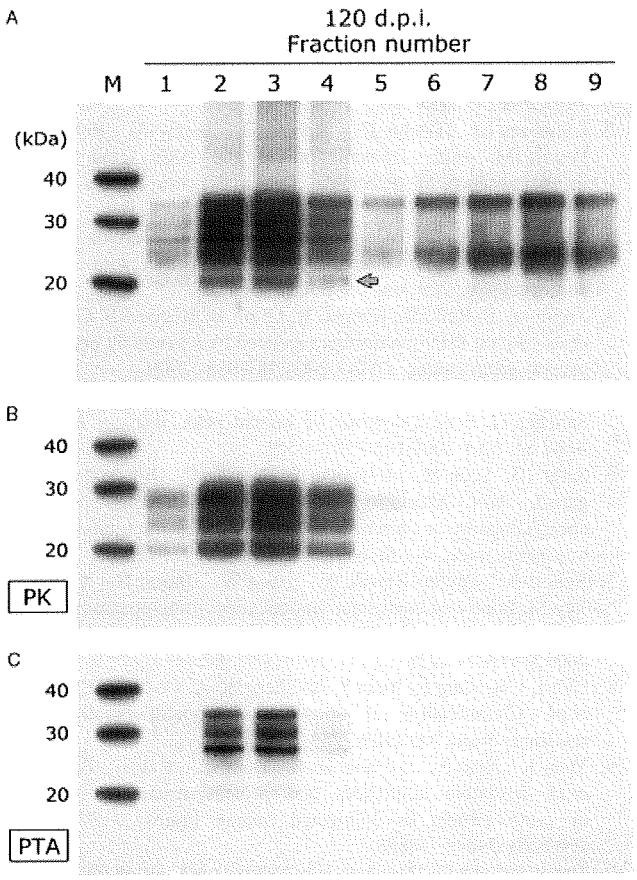

Figure 5. Characteristics of PrP oligomers at the terminal disease stage. (A) Another experiment of PrP fractionation for the sample at 120 days post-inoculation, which reproduces the results shown in Figure 3B. Note that PrP oligomers in fractions 1–4 involved PrP^{res}-like fragments, of which the non-glycosylated form was around 21 kDa (grey arrow), as also shown in Figure 6. (B) The fractions were treated with PK to detect PrP^{res} in each fraction. (C) PTA precipitation was conducted for each fraction. M, molecular weight markers. PK digestion and PTA precipitation were conducted for the same amount of each fraction applied in (A). PrP oligomers in fractions 1–4 were PK-resistant and PTA-precipitable, even though the retrieved PrP molecules by PTA precipitation were apparently less than those in the original fractions. PK, proteinase-K treatment; PTA, phosphotungstic acid precipitation

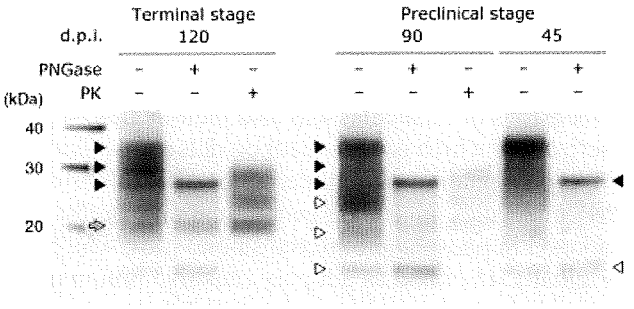

Figure 6. Comparison of the migration pattern and glycoform pattern of PrP between the terminal stage and the preclinical stage. A western blot is shown for PrP treated with or without PK or PNGase at the indicated time points. Total PrP in preclinical stages consisted of full-length molecules (black triangles) and the smaller fragments whose molecular size was different from PrP^{res} (open triangles). PNGase deglycosylation unambiguously showed the non-glycosylated form of each PrP molecule. PrP^{res}-like fragments were also detected at the terminal stage, of which the non-glycosylated form was around 21 kDa (grey arrow). Three glycoform bands of PrP^{res} at 120 days post-inoculation (d.p.i.) showed almost even densities, whereas the di-glycosylated band was prominent in PK-sensitive PrP in preclinical stages. PNGase, peptide-N-glycosidase treatment; PK, proteinase-K treatment

than the peak observed by western blot analyses (cf. Figures 4B and 3B). Fractions 2 and 3 could also contain highly aggregated fibrils; however, substantial quantities of PrP fibrils might have been trapped in the gel beds, because smaller amounts of PrP molecules were retrieved from the fractionated samples by PTA precipitation than expected. Therefore, a further experiment to measure the molecular size of PrP molecules in these fractions is required. Although sucrose gradient sedimentation could be more suitable for detecting total PrP fibrils [8,9], the more easily applicable gel-filtration method described in this study would benefit research on protein oligomers. This method is also applicable to human materials [31] and may be useful in addressing regional differences in the brain.

Levels of PrP oligomers increase with disease progression in the NZW/Fukuoka-1 mouse model of TSE, which precedes the appearance of PrP^{res}. In the early disease stage, PK-sensitive, PTA-soluble PrP oligomers might affect the disease pathology, such as spongiform change and abnormal PrP deposition. Although biochemical analyses for the whole brain homogenates may not exactly correlate with local pathological changes, the increase of oligomeric PrP was related to the exacerbation of spongiform change. PrP oligomers subsequently develop PK resistance and insolubility in PTA precipitation, and PrP^{res}-like fragments derived from putative endogenous proteolysis are also evident in the terminal stage. It is known that the turnover of PrP^{C} and of PrP^{res} are quite different [32] and, accordingly, developing PrP oligomers would have intermediate half-lives, dependent upon their degree of protease resistance. In addition, the shift of glycosylation ratio is associated with the development of PK resistance. The 'underglycosylated PrP species' as an early biochemical fingerprint of PrP^{Sc} infection has been reported by Pan *et al* [33]; however, highly glycosylated PrP could also form abnormal oligomers at 90 days post-inoculation in our study. This suggests that PrP oligomers are not clearly distinguished from PrP^{C} or PrP^{res} but may overlap in a continuous spectrum.

The PrP bands differed in patterns among the three time points, as shown in Figure 3B. It should also be noted that the major band in 90 day samples was similar in size to the monoglycosylated form of PrP^{res}. However, PNGase deglycosylation revealed that the major molecules at 90 days should be the diglycosylated form of endogenously truncated PrP. These truncated fragments were also seen in 45 day and control samples, which were certainly PK-sensitive. The reason why the proportion of truncated fragments differed among each time point is still unclear; although it is possible that endogenous protease activity and/or

protease sensitivity of PrP may vary according to the age and/or disease progression.

Size-exclusion gel chromatography measures the dimensions of molecules and also their degree of polymerization, which is dependent on detergent solubility. PTA precipitation also determines the solubility of PrP molecules in a detergent-containing buffer (2% sarkosyl in phosphate-buffered saline) [28], which was originally described as a highly sensitive immunoblotting assay for the detection of PrP^{Sc} because this method involves the enrichment effect. In the present study we avoided the enrichment of PrP^{Sc} so that PTA solubility of fractionated PrP could be simply determined. The extracted oligomers in this gel-filtration method showed a certain degree of PTA solubility, which might be due to the relatively intense detergent conditions in PTA-precipitation procedures. Indeed, varying SDS concentrations may influence the conformation and polymeric state of PrP [34]. Although these experimental conditions are certainly different from physiological states, PrP oligomers retained the acquired property of detergent insolubility even after freeze–thaw cycles (Figures 3B, 5A).

The definition of PrP^{Sc} should differ depending on whether PrP molecules are classified based on their polymeric state or on PK resistance. Moreover, detergent solubility can be affected by different experimental conditions and, in particular, PTA precipitation might be insufficient to detect PrP oligomers in some cases. Further investigations, including transmission and neurotoxicity studies, are required to determine which property is critical for the pathogenesis of PrP^{Sc}. Protein misfolding cyclic amplification assay (PMCA) might be also useful to examine whether prepared PrP molecules are capable of promoting conversion of PrP^{C} into PrP^{Sc} [35,36].

In conclusion, the novel spin-column gel filtration method was able to detect PrP oligomers in a TSE mouse model preceding the accumulation of PrP^{res}, and clearly demonstrated the development of PrP^{Sc}. Not only the polymeric state but also both PK resistance and PTA insolubility of PrP oligomers were intensified with disease progression. It would be highly recommended that the abnormality of PrP molecules should be determined from various perspectives more than protease resistance. Our study casts light on the ambiguity of the definition of PrP^{Sc}, which requires further investigations of disease-associated PrP isoforms that result in neurodegeneration and prion propagation.

Acknowledgements

This study was supported by Grants-in-Aid for Scientists from the Ministry of Health, Labour and Welfare, Japan (H19-nanchi-ippan-006) and by the Japan Society for the Promotion of Science (No. 19500309). We thank Ms S Nagae and Ms K Satoh for their excellent technical assistance.

References

1. Prusiner SB. Prion diseases and the BSE crisis. *Science* 1997;**278:**245–251.
2. Lasmezas CI, Deslys JP, Robain O, Jaegly A, Beringue V, Peyrin JM, *et al.* Transmission of the BSE agent to mice in the absence of detectable abnormal prion protein. *Science* 1997;**275:**402–405.
3. Safar J, Wille H, Itri V, Groth D, Serban H, Torchia M, *et al.* Eight prion strains have PrP^{Sc} molecules with different conformations. *Nat Med* 1998;**4:**1157–1165.
4. Tremblay P, Ball HL, Kaneko K, Groth D, Hegde RS, Cohen FE, *et al.* Mutant PrP^{Sc} conformers induced by a synthetic peptide and several prion strains. *J Virol* 2004;**78:**2088–2099.
5. Safar JG, Geschwind MD, Deering C, Didorenko S, Sattavat M, Sanchez H, *et al.* Diagnosis of human prion disease. *Proc Natl Acad Sci USA* 2005;**102:**3501–3506.
6. Safar JG, Scott M, Monaghan J, Deering C, Didorenko S, Vergara J, *et al.* Measuring prions causing bovine spongiform encephalopathy or chronic wasting disease by immunoassays and transgenic mice. *Nat Biotechnol* 2002;**20:**1147–1150.
7. Bellon A, Seyfert-Brandt W, Lang W, Baron H, Groner A, Vey M. Improved conformation-dependent immunoassay: suitability for human prion detection with enhanced sensitivity. *J Gen Virol* 2003;**84:**1921–1925.
8. Cali I, Castellani R, Yuan J, Al-Shekhlee A, Cohen ML, Xiao X, *et al.* Classification of sporadic Creutzfeldt–Jakob disease revisited. *Brain* 2006;**129:**2266–2277.
9. Yuan J, Xiao X, McGeehan J, Dong Z, Cali I, Fujioka H, *et al.* Insoluble aggregates and protease-resistant conformers of prion protein in uninfected human brains. *J Biol Chem* 2006;**281:**34848–34858.
10. Tcherkasskaya O, Davidson EA, Schmerr MJ, Orser CS. Conformational biosensor for diagnosis of prion diseases. *Biotechnol Lett* 2005;**27:**671–675.
11. Birkmann E, Schafer O, Weinmann N, Dumpitak C, Beekes M, Jackman R, *et al.* Detection of prion particles in samples of BSE and scrapie by fluorescence correlation spectroscopy without proteinase K digestion. *Biol Chem* 2006;**387:**95–102.
12. Vasan S, Mong PY, Grossman A. Interaction of prion protein with small highly structured RNAs: detection and characterization of PrP-oligomers. *Neurochem Res* 2006;**31:**629–637.
13. McLean CA, Cherny RA, Fraser FW, Fuller SJ, Smith MJ, Beyreuther K, *et al.* Soluble pool of Aβ amyloid as a determinant of severity of neurodegeneration in Alzheimer's disease. *Ann Neurol* 1999;**46:**860–866.
14. Walsh DM, Klyubin I, Fadeeva JV, Cullen WK, Anwyl R, Wolfe MS, *et al.* Naturally secreted oligomers of amyloid β protein potently inhibit hippocampal long-term potentiation *in vivo*. *Nature* 2002;**416:**535–539.
15. Kaylor J, Bodner N, Edridge S, Yamin G, Hong DP, Fink AL. Characterization of oligomeric intermediates in α-synuclein fibrillation: FRET studies of Y125W/Y133F/Y136F α-synuclein. *J Mol Biol* 2005;**353:**357–372.
16. Takahashi Y, Okamoto Y, Popiel HA, Fujikake N, Toda T, Kinjo M, *et al.* Detection of polyglutamine protein oligomers in cells by fluorescence correlation spectroscopy. *J Biol Chem* 2007;**282:**24039–24048.
17. Lashuel HA, Hartley D, Petre BM, Walz T, Lansbury PT Jr. Neurodegenerative disease: amyloid pores from pathogenic mutations. *Nature* 2002;**418:**291.
18. Singer SJ, Dewji NN. Evidence that Perutz's double-β-stranded subunit structure for β-amyloids also applies to their channel-forming structures in membranes. *Proc Natl Acad Sci USA* 2006;**103:**1546–1550.
19. Caughey B, Lansbury PT. Protofibrils, pores, fibrils, and neurodegeneration: separating the responsible protein aggregates from the innocent bystanders. *Annu Rev Neurosci* 2003;**26:**267–298.
20. Wille H, Michelitsch MD, Guenebaut V, Supattapone S, Serban A, Cohen FE, *et al.* Structural studies of the scrapie prion protein by electron crystallography. *Proc Natl Acad Sci USA* 2002;**99:**3563–3568.

21. Yang S, Levine H, Onuchic JN, Cox DL. Structure of infectious prions: stabilization by domain swapping. *FASEB J* 2005;**19:**1778–1782.
22. Lin MC, Mirzabekov T, Kagan BL. Channel formation by a neurotoxic prion protein fragment. *J Biol Chem* 1997;**272:**44–47.
23. Silveira JR, Raymond GJ, Hughson AG, Race RE, Sim VL, Hayes SF, *et al*. The most infectious prion protein particles. *Nature* 2005;**437:**257–261.
24. Kazlauskaite J, Young A, Gardner CE, Macpherson JV, Venien-Bryan C, Pinheiro TJ. An unusual soluble β-turn-rich conformation of prion is involved in fibril formation and toxic to neuronal cells. *Biochem Biophys Res Commun* 2005;**328:**292–305.
25. Simoneau S, Rezaei H, Sales N, Kaiser-Schulz G, Lefebvre-Roque M, Vidal C, *et al*. *In vitro* and *in vivo* neurotoxicity of prion protein oligomers. *PLoS Pathog* 2007;**3:**1175–1186.
26. Tateishi J, Ohta M, Koga M, Sato Y, Kuroiwa Y. Transmission of chronic spongiform encephalopathy with kuru plaques from humans to small rodents. *Ann Neurol* 1979;**5:**581–584.
27. Sasaki K, Doh-ura K, Ironside J, Mabbott N, Iwaki T. Clusterin expression in follicular dendritic cells associated with prion protein accumulation. *J Pathol* 2006;**209:**484–491.
28. Wadsworth JD, Joiner S, Hill AF, Campbell TA, Desbruslais M, Luthert PJ, *et al*. Tissue distribution of protease resistant prion protein in variant Creutzfeldt–Jakob disease using a highly sensitive immunoblotting assay. *Lancet* 2001;**358:**171–180.
29. Kayed R, Head E, Thompson JL, McIntire TM, Milton SC, Cotman CW, *et al*. Common structure of soluble amyloid oligomers implies common mechanism of pathogenesis. *Science* 2003;**300:**486–489.
30. Jimenez-Huete A, Lievens PM, Vidal R, Piccardo P, Ghetti B, Tagliavini F, *et al*. Endogenous proteolytic cleavage of normal and disease-associated isoforms of the human prion protein in neural and non-neural tissues. *Am J Pathol* 1998;**153:**1561–1572.
31. Minaki H, Sasaki K, Honda H, Iwaki T. Prion protein oligomers in Creutzfeldt–Jakob disease detected by gel-filtration centrifuge columns. *Neuropathology* 2009;DOI:10.1111/j.1440-1789.2009.01007.x.
32. Borchelt DR, Scott M, Taraboulos A, Stahl N, Prusiner SB. Scrapie and cellular prion proteins differ in their kinetics of synthesis and topology in cultured cells. *J Cell Biol* 1990;**110:**743–752.
33. Pan T, Wong P, Chang B, Li C, Li R, Kang SC, *et al*. Biochemical fingerprints of prion infection: accumulations of aberrant full-length and N-terminally truncated PrP species are common features in mouse prion disease. *J Virol* 2005;**79:**934–943.
34. Riesner D. Biochemistry and structure of PrP^{C} and PrP^{Sc}. *Br Med Bull* 2003;**66:**21–33.
35. Saborio GP, Permanne B, Soto C. Sensitive detection of pathological prion protein by cyclic amplification of protein misfolding. *Nature* 2001;**411:**810–813.
36. Pastrana MA, Sajnani G, Onisko B, Castilla J, Morales R, Soto C, *et al*. Isolation and characterization of a proteinase K-sensitive PrP^{Sc} fraction. *Biochemistry* 2006;**45:**15710–15717.

Cell Death and Differentiation (2009) 16, 1315–1322

www.nature.com/cdd

ITPase-deficient mice show growth retardation and die before weaning

M Behmanesh[1,2], K Sakumi*[,1], N Abolhassani[1], S Toyokuni[3], S Oka[1], YN Ohnishi[1], D Tsuchimoto[1] and Y Nakabeppu[1]

Inosine triphosphate pyrophosphatase (ITPase), the enzyme that hydrolyzes ITP and other deaminated purine nucleoside triphosphates to the corresponding purine nucleoside monophosphate and pyrophosphate, is encoded by the *Itpa* gene. In this study, we established *Itpa* knockout (KO) mice and used them to show that ITPase is required for the normal organization of sarcomeres in the heart. *Itpa*$^{-/-}$ mice died about 2 weeks after birth with features of growth retardation and cardiac myofiber disarray, similar to the phenotype of the cardiac α-actin KO mouse. Inosine nucleotides were found to accumulate in both the nucleotide pool and RNA of *Itpa*$^{-/-}$ mice. These data suggest that the role of ITPase in mice is to exclude ITP from the ATP pool, and the main target substrate of this enzyme is rITP. Our data also suggest that cardiomyopathy, which is mainly caused by mutations in sarcomeric protein-encoding genes, is also caused by a defect in maintaining the quality of the ATP pool, which is an essential requirement for sarcomere function.
Cell Death and Differentiation (2009) **16,** 1315–1322; doi:10.1038/cdd.2009.53; published online 5 June 2009

Nucleotide and polynucleotide molecules are spontaneously damaged under the physiological conditions.[1–3] These modifications often cause a nucleotide to pair with an alternate partner nucleotide in DNA.[4,5] For example, 8-oxo-dGTP, an oxidized product of dGTP, can pair with adenine as well as cytosine during replication, resulting in a transversion mutation.[4] 8-Oxoguanine in DNA appears through two independent pathways, either by an incorporation of the oxidized precursor, 8-oxo-dGTP during DNA synthesis, or by the direct oxidation of a guanine base in DNA.[6,7] To prevent the former pathway from being used, mammals possess the oxidized purine nucleoside triphosphatase encoded by the *Mth1* gene, that degrades 8-oxo-dGTP into 8-oxo-dGMP and pyrophosphate,[8,9] and to protect against the latter pathway, 8-oxoguanine-DNA glycosylase, encoded by the *Ogg1* gene, removes the oxidized base from the DNA.[10–15] To evaluate the roles of these enzymes in mouse, we produced *Ogg1* and *Mth1* single-knockout mice, as well as *Ogg1* plus *Mth1* double-knockout mice, and showed their tumor susceptibility and the accumulation of 8-oxoguanine in their DNA.[6]

Similar to oxidation, deamination is also a common chemical modification that nucleotides may undergo under physiological conditions.[1,2] In the case of deaminated purine bases, such as hypoxanthine, it is considered that inosine triphosphate pyrophosphatase (ITPase), endonuclease V and hypoxanthine-DNA glycosylase have a role in eliminating the deaminated bases from DNA.[16–19] Saparbaev and Laval[19] reported that alkylpurine-DNA glycosylases engage in hypoxanthine-DNA glycosylase activity both in *Escherichia coli* and mammalian cells. The alkylpurine-DNA glycosylase-deficient (*Mpg* knockout) mouse has features of impaired base excision repair of alkylation-induced DNA damage, and increased sensitivity to methyl methanesulfonate and streptozotocin-induced diabetes.[20,21] However, there is no report regarding ITPase and endonuclease V knockout mouse as yet.

The enzyme activity of ITPase (EC 3.6.1.19) was first described in 1969.[22] ITPase, which is encoded by the *Itpa* gene in mammals, hydrolyzes deaminated purine nucleoside triphosphates, such as dITP and ITP, to the corresponding purine nucleoside monophosphate and pyrophosphate.[16,23] The enzyme was identified as a novel NTP pyrophosphatase by a protein structure-based approach in 1999.[24] We have reported the genomic organization and expression of the mouse *Itpa* gene in 2005.[23] In this study to elucidate the biological significance of ITPase in mice, we produced an *Itpa* knockout. These *Itpa*$^{-/-}$ mice died about 2 weeks after birth with features of growth retardation and cardiac myofiber disarray.

Results

Biological features of *Itpa*$^{-/-}$ mice. To disrupt the *Itpa* gene, exons 2–4 that encode V23-I88 of mouse ITPase were replaced with the *polII-neo* cassette (Figure 1a). Two independently targeted ES clones were obtained and used to establish the knockout (KO) mouse strains. The *Itpa* gene-disrupted ES cells were injected into C57BL/6J blastocysts to produce *Itpa* KO mice. Disruption of the *Itpa* gene was confirmed by Southern blotting (ES clone, Figure 1b) as well as by genomic PCR (KO mice, Figure 1c). When we analyzed the expression of the *Itpa* gene in *Itpa* KO mice,

[1]Division of Neurofunctional Genomics, Department of Immunobiology and Neuroscience, Medical Institute of Bioregulation, Kyushu University, Fukuoka 812-8582, Japan; [2]Department of Genetics, School of Sciences, Tarbiat Modares University, PO Box 14115-175, Tehran, Iran and [3]Department of Pathology and Biological Responses, Graduate School of Medicine, Nagoya University, Nagoya 466-8550, Japan
*Correspondence: K Sakumi, Division of Neurofunctional Genomics, Department of Immunobiology and Neuroscience, Medical Institute of Bioregulation, Kyushu University, 3-1-1 Maidashi, Higashi-Ku, Fukuoka, Fukuoka 812-8582, Japan. Tel: +81 92 642 68 02; Fax: +81 92 642 68 04; E-mail: sakumi@bioreg.kyushu-u.ac.jp
Keywords: ITPase; nucleotide pool; ATP; mouse mutant; cardiomyopathy
Abbreviations: ITPase, inosine triphosphate pyrophosphatase; RBCs, red blood cells; KO, knockout
Received 24.9.08; revised 10.3.09; accepted 15.4.09; Edited by M Piacentini; published online 05.6.09

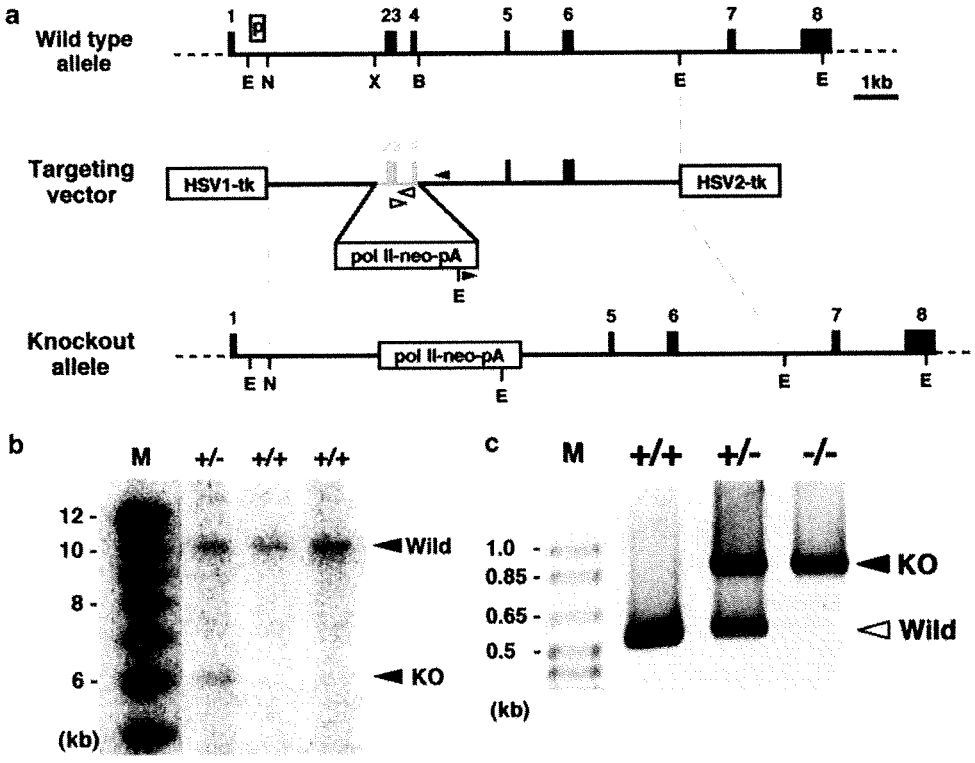

Figure 1 Generation of the *Itpa*$^{-/-}$ mouse. (**a**) Schematic representation of a partial restriction map of the mouse *Itpa* locus, targeting vector and targeted allele. PCR primers to detect the wild type and knockout alleles are indicated by open and closed triangles, respectively. 'p' indicates the probe fragment used in Southern blot analysis. As there are several *Itpa* pseudogenes in the mouse genome,[23] we cloned the exact *Itpa* gene located on chromosome 2 and used it to construct a targeting vector. (**b**) Southern blot analysis of *Itpa*$^{+/-}$ ES cells. The 5′-flanking probe (p) was used to distinguish the *Eco*RI-digested targeted allele. An approximate 6 kb targeted allele (KO) was found only in the lane of *Itpa*$^{+/-}$ ES cells. (**c**) Targeted allele confirmed by the genomic PCR of mouse tail DNA. Amplified DNAs derived from wild type (WT) and knockout (KO) alleles are indicated by open and closed triangles, respectively

we detected a shorter length of cDNA in the RT-PCR product of *Itpa* KO mouse RNAs using primer sets positioned in exons 1 and 8 (Figure 2a). The shorter length of cDNA was detected in both KO mouse strains. The unexpected cDNA contained a sequence corresponding to exons 1, 5, 6, 7 and 8, with one G insertion between exons 1 and 5 (Figure 2b). This abnormally spliced RNA encodes a polypeptide composed of 29 amino acids, that is, the first 22 amino acids encoded by exon 1 of the *Itpa* gene and an additional 7 misframed amino acids derived from the exon 5 sequence. The aberrant translation product lacks the major portion of ITPase (176 a.a./198 a.a.), including the residues thought to interact with ITP (Figure 2c).[16] The null expression of the ITPase protein in the *Itpa*$^{-/-}$ mouse was confirmed by western blotting using a rabbit anti-ITPase antiserum. We did not detect any signal corresponding to the expected size of ITPase (MW, 21.9 kDa) in *Itpa*$^{-/-}$ mouse samples (Figure 3a). A 3.1 kDa peptide, the expected translation product of abnormally spliced RNA, was not detected in our system, perhaps because of an instability of the peptide or the detection limit of the antiserum (Supplementary Figure). Finally, no ITPase activity was detected in the erythrocyte extract of the *Itpa*$^{-/-}$ mouse (Figure 3b), and we concluded that the gene disruption had succeeded.

The *Itpa*$^{+/-}$ mouse was indistinguishable from its *Itpa*$^{+/+}$ littermates with respect to size, viability, fertility and behavior. About 10% of offspring obtained by the mating of *Itpa*$^{+/-}$ mice showed the *Itpa*$^{-/-}$ genotype (Figure 4a). The birth ratio indicates that more than half of the *Itpa*$^{-/-}$ mice died before birth. Although there was a significant amount of milk in the stomach of *Itpa*$^{-/-}$ newborn mice, these mice showed growth retardation and died about 14 days after birth (Figure 4b-d). Prior to death, the *Itpa*$^{-/-}$ mouse showed ataxia, abnormal breathing (Supplemental Movie 1) and heart abnormalities. These phenotypes were common in the two knockout mouse lines, independently established from different *Itpa*$^{+/-}$ ES cells. On pathological analysis, the *Itpa*$^{-/-}$ mouse showed such features as immature hair follicles, hyperkeratosis of the forestomach, decreased extramedullary hematopoiesis in liver and spleen, and germ cell hypoplasia in testis (data not shown), in addition to hypoplasia of the heart (Figure 5a-c). The heart of the *Itpa*$^{-/-}$ mouse was smaller and immature, especially the ventricle regions. Analysis of a 10 days old *Itpa*$^{-/-}$ mouse heart showed that both ventricular chamber walls were thinner than those of the *Itpa*$^{+/+}$ mouse heart (Figure 5d-f). The striated staining of desmin corresponding to the Z-disc was absent in the *Itpa*$^{-/-}$ heart and disorganization of myocardial fiber was observed (Figure 5g-i). By ultrastructural analysis of *Itpa*$^{-/-}$ mouse cardiomyocytes, it was evident that the number of sarcomeres was decreased and that the sarcomere structure was broken and disorganized. The shape of mitochondria was changed, although the inner

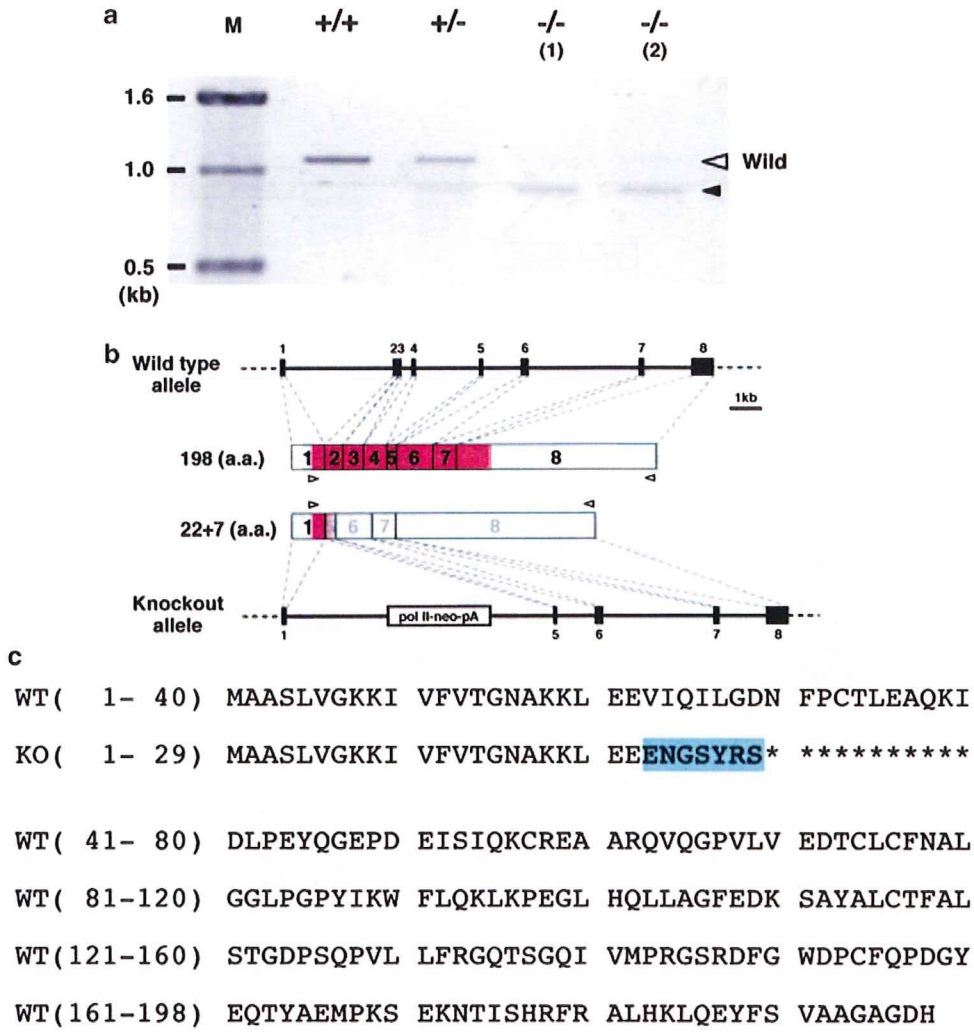

Figure 2 RT-PCR analysis of *Itpa*$^{-/-}$ mouse RNA. (**a**) An aberrant RNA transcribed from the targeted allele. Positions of the primers used in the RT-PCR are shown in Figure 2b. The length of cDNA expected from the wild-type allele is shown with an open triangle, and the unexpected cDNA from the targeted allele, with a closed triangle. (1) and (2) indicate the different KO mouse strains. cDNAs prepared from the liver RNA were shown. The shorter molecule was also observed in the heart cDNA of the *Itpa*$^{-/-}$ mouse (data not shown). (**b**) An aberrant transcript encodes a short peptide composed of 29 amino acids. Amino acid sequences predicted from the nucleotide sequence of RT-PCR products and the predicted splicing occurring in wild and *Itpa*$^{-/-}$ mice are presented. Positions of the primers used in the RT-PCR are shown by open triangles. Peptide coding regions are shown in magenta. (**c**) Comparison of the predicted amino-acid sequence between wild-type ITPase and the short peptide encoded by the aberrant mRNA transcribed from the targeted allele. In the amino-acid sequence of the short peptide from *Itpa*$^{-/-}$ mouse cDNA, frame-shifted amino acids are indicated in the blue area

and outer membrane structure seemed normal (Figure 5j-l). We detected neither apoptotic cardiomyocytes nor symptoms of myocardial infarction in *Itpa*$^{-/-}$ mouse heart (data not shown). These results indicate that an ITPase deficiency causes disruption of the sarcomere structure in cardiomyocytes. Using echocardiography, we compared the cardiac performance of the *Itpa*$^{-/-}$ mouse to that of the wild type. As shown in Supplementary Movie 2, movement of the *Itpa*$^{-/-}$ mouse heart was unsynchronized and jerky.

Accumulation of inosine nucleotides in the *Itpa*$^{-/-}$ mouse. Under ITPase-deficient conditions, ITP was expected to appear in the nucleotide pool and the accumulated ITP to be incorporated into RNA. To analyze the contents of the nucleotide pool, we set up nucleotide separation conditions under which 15 kinds of nucleotides (ATP, CTP, GTP, UTP, ITP and their mono- and diphosphate forms) could be separated using an HPLC system equipped with a C-18 column (Figure 6a). As shown in Figure 6b, we confirmed that the ITP accumulation corresponded to about 10% of the ATP molecules in the nucleotide pool of the *Itpa*$^{-/-}$ mouse (10 days old) erythrocytes. No ITP was detected in *Itpa*$^{+/+}$ and *Itpa*$^{+/-}$ mouse erythrocytes. In the case of organs, including the heart, however, we could not detect any ITP peak in the nucleotide pool of the *Itpa*$^{-/-}$ mouse (data not shown). One possibility is that the accumulated ITP is spent in its incorporation into RNA by transcription, except in erythrocytes where transcription does not occur. Alternatively, a rapid degradation of nucleotides may prevent detection of minor nucleotide species in tissues.

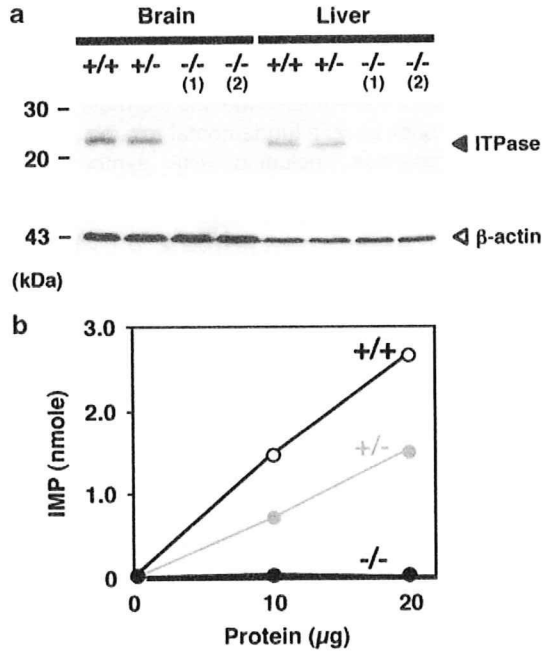

Figure 3 (**a**) Western blot analysis of *Itpa*$^{-/-}$ mouse tissues. ITPase is indicated by a closed triangle. (1) and (2) indicate the different KO mouse strains. Full imaging of the blot is shown in the Supplementary Figure with a long exposed image. (**b**) No ITPase activity was detected in the erythrocyte extract of the *Itpa*$^{-/-}$ mouse. The amount of IMP released from ITP by the erythrocyte extract was determined by HPLC as described in the Materials and Methods section. *Itpa*$^{+/+}$, open circle; *Itpa*$^{+/-}$, gray circle; *Itpa*$^{-/-}$, closed circle

To determine the inosine nucleotide that was incorporated into RNA, we digested total heart RNA with the nuclease P1, and separated the digest on a C-18 column. As shown in Figure 6c, we detected IMP in *Itpa*$^{-/-}$ mouse RNA, and the amount was equivalent to about 1% of the AMP. These results clearly showed that ITP was produced in mouse cells, and that ITPase degraded the deaminated nucleotides to maintain the quality of the ATP pool.

Expression of the *Actc1* gene in *Itpa*$^{-/-}$ mouse. As shown in Figure 5j, it was evident that the number of sarcomeres was decreased and that the sarcomere structure was broken and disorganized. This kind of abnormality is also a feature of human cardiomyopathy and its mouse models.[29] Although a number of genes have been identified as responsible for the cardiomyopathy,[30] until now, the *Itpa* gene has not been reported as a candidate.

A deficiency in the *Actc1* gene, one of the genes encoding sarcomeric protein, is a causative factor of human cardiomyopathy. This gene encodes cardiac α-actin, and the *Actc1* knockout mouse showed a similar phenotype to that of the *Itpa*$^{-/-}$ mouse.[31] As the *Actc1* gene is located near the *Itpa* gene on mouse chromosome 2, we determined whether *Itpa* gene disruption affected *Actc1* gene expression. Semiquantitative RT-PCR analysis showed that the amount of *Actc1* mRNA was not affected by *Itpa* gene disruption in the heart (Figure 7). The nucleotide sequence of *Actc1* cDNA cloned from *Itpa*$^{-/-}$ mouse heart showed no mutations (data not

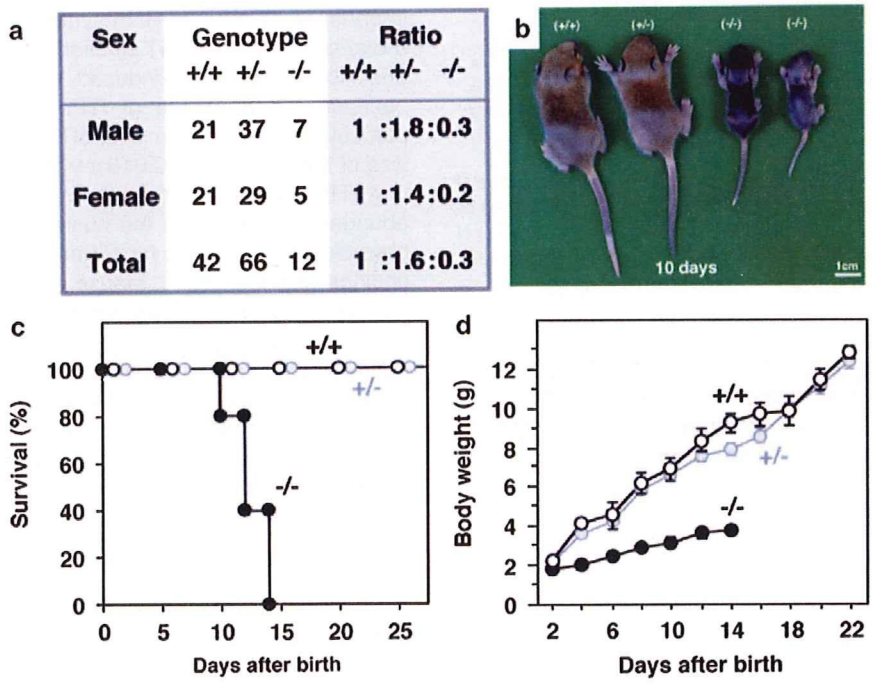

Figure 4 *Itpa*$^{-/-}$ mice died before weaning. (**a**) The birth ratio of the *Itpa*$^{-/-}$ mouse was not in accordance with the Mendel's laws. To determine the birth ratio of the *Itpa*$^{-/-}$ mouse, *Itpa*$^{+/-}$ mice (N1), which were the offspring of chimera male mice and C57BL/6J females, were used for mating. (**b**) *Itpa*$^{-/-}$ mice were smaller than *Itpa*$^{+/+}$ and *Itpa*$^{+/-}$ mice. Ten days old male mice from the same litter were compared. (**c**) *Itpa*$^{-/-}$ mice died about 2 weeks after birth. The survival curve is shown as a Kaplan–Meier's plot. *Itpa*$^{+/+}$, open circle; *Itpa*$^{+/-}$, gray circle; *Itpa*$^{-/-}$, closed circle. (**d**) *Itpa*$^{-/-}$ mice showed growth retardation. *Itpa*$^{+/+}$, open circle; *Itpa*$^{+/-}$, gray circle; *Itpa*$^{-/-}$, closed circle. Error bar, S.E.M

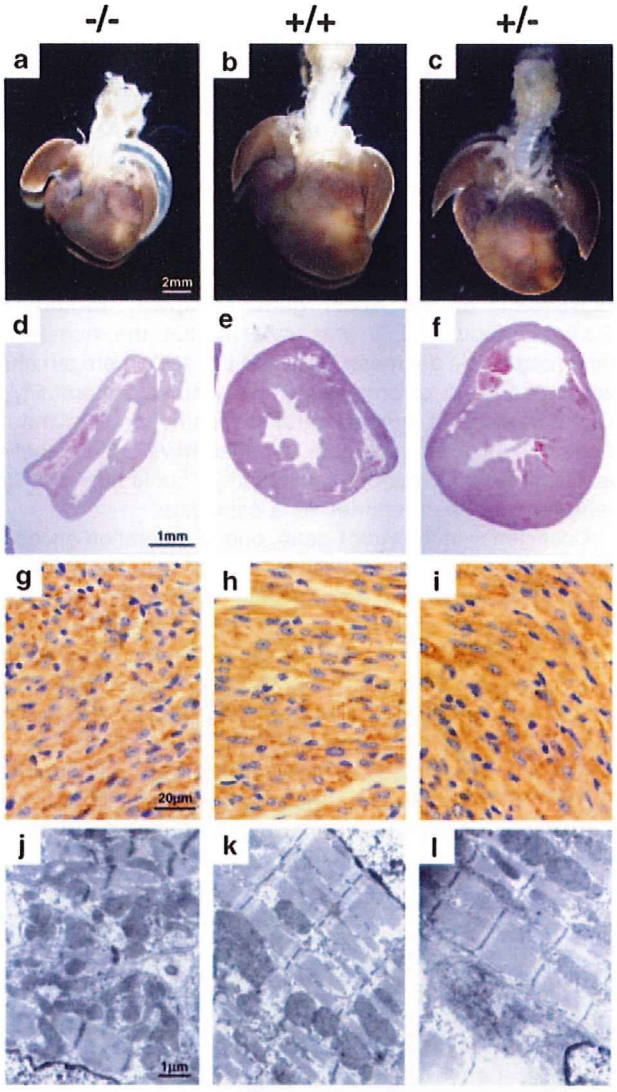

Figure 5 The *Itpa*$^{-/-}$ mouse showed heart abnormalities. (**a–c**) Hypoplasia of *Itpa*$^{-/-}$ mouse heart (10 days old). (**d–f**) A horizontal section of heart stained by hematoxylin and eosin (11 days old). (**g–i**) Desmin staining. The Z-disc was not observed in the *Itpa*$^{-/-}$ mouse (11 days old). (**j–l**) Electron micrographic analysis. Microfibrillar disarray was evident in *Itpa*$^{-/-}$ mouse heart (10 days old)

shown). These results support the concept that the presence of ITP in the ATP pool has a deleterious effect on sarcomeric proteins, such as actomyosin, and that ITPase activity may alter vulnerability to certain cardiac muscle diseases.

Discussion

To control the quality of the nucleotide pool, organisms possess a number of nucleoside triphosphatases, which degrade non-canonical nucleoside triphosphates.[32] To clarify the biological significance of the damaged nucleotides and the enzymes that eliminate them, we produced and analyzed KO mice which lack sanitizing enzyme activity. Here, we have produced and analyzed ITPase-deficient (*Itpa*$^{-/-}$) mice. In contrast to the *Mth1*$^{-/-}$ mouse, which lacks 8-oxo-dGTPase activity and survives normally, the *Itpa*$^{-/-}$ mouse dies before weaning with features of growth retardation. We found that the heart of the *Itpa*$^{-/-}$ mouse is structurally and functionally abnormal.

ATP, a multifunctional nucleotide and the most abundant in the nucleotide pool, plays a fundamental role in a wide variety of cellular processes, including RNA synthesis, energy translation, signal transduction, cytoskeleton remodeling and muscle contraction. In the case of cardiac function, a number of sarcomere proteins require ATP for their normal activities. Oxidative deamination of adenine at C-6 converts ATP to ITP. Because ITP retains a molecular structure similar to that of ATP, it can act as an aberrant substrate replacing ATP in some biological processes. For example, it has been shown that Mg•ITP-bound actomyosin has a greatly reduced shortening velocity and rate of force recovery as compared with the Mg•ATP-bound form, and shows disordered striations during activation *in vitro*.[33] One likely possibility is that, during cardiac development of the *Itpa*$^{-/-}$ mouse, accumulated ITP competes with ATP (Figure 8a), which is required for actomyosin function in the sarcomere. Asynchronous sarcomere movements may cause a degradation of the striated pattern of the sarcomere, and destroy its well-organized structure (Figure 5j), which is essential for heart function. In addition, we observed that IMP is accumulated in the RNA of *Itpa*$^{-/-}$ mouse tissue (Figure 6c). It is also likely that the incorporated hypoxanthine nucleotides cause RNA information to be altered, resulting in the production of defective proteins and destruction of the structure of functional RNAs. In either case, it is necessary for cells to eliminate ITP from their ATP pool by ITPase to keep themselves healthy.

It is well known that quality control of the nucleotide pool is important for DNA and RNA synthesis. By way of analogy to 8-oxo-dGTPase (MTH1) function, ITPase has been considered to prevent dITP-induced mutagenesis.[7,16] However, because the K_m value of ITPase to its substrate is not particularly small (0.31 mM for dITP), [16] as compared with the size of the dNTP pool (0.013 mM for dATP),[34] it is more likely that ITP, a deaminated product of ATP, which is the most abundant nucleotide in the nucleotide pool (2.8 mM),[34] is a physiological substrate for ITPase in mammalian cells. Our findings with the *Itpa*$^{-/-}$ mouse are in good agreement with the hypothesis that ITPase functions to exclude ITP from the ATP pool and to protect cells from the harmful influence of deaminated purine nucleotides (Figure 8b).

In the case of human ITPase deficiencies, however, no major phenotype except for the abnormal accumulation of ITP in erythrocytes has been reported. Sumi *et al.*[35,36] found that the P32T mutation is responsible for the human ITPase deficiency, and proposed a relationship between this deficiency and an increased sensitivity to the toxicity of purine analog drugs. They mentioned that the ITP level in ITPase-deficient human erythrocytes may represent 10–25% of the ATP pool, which is similar to the amount of ITP observed in the *Itpa*$^{-/-}$ mouse. To explain the difference in the phenotypes of ITPase-deficient mice and humans, we considered two hypotheses. One is that there is another compensational mechanism in human cells used in excluding ITP from the ATP pool, other than that involving ITPase. The other is that an ITPase deficiency may be related to some form of heart

disease in human populations, although this possibility has not yet been sufficiently explored. Clinical and biochemical analyses of ITPase-deficient patients may provide an answer.

As observed in the *Itpa*$^{-/-}$ mouse, a loss in ITP degradation leads to a cardiomyopathy-like phenotype, which is mainly caused by mutations of sarcomeric protein-encoding genes. It is clear that maintenance of the quality of the ATP pool is important for sarcomere organization in the heart. As ITP has structural similarity not only to ATP but also to GTP, ITPase activity would be important in keeping biochemical processes in cells functioning properly. Using ITPase-deficient cells, we are now able to evaluate the significance of deaminated purine nucleoside triphosphates originating in mammalian cells.

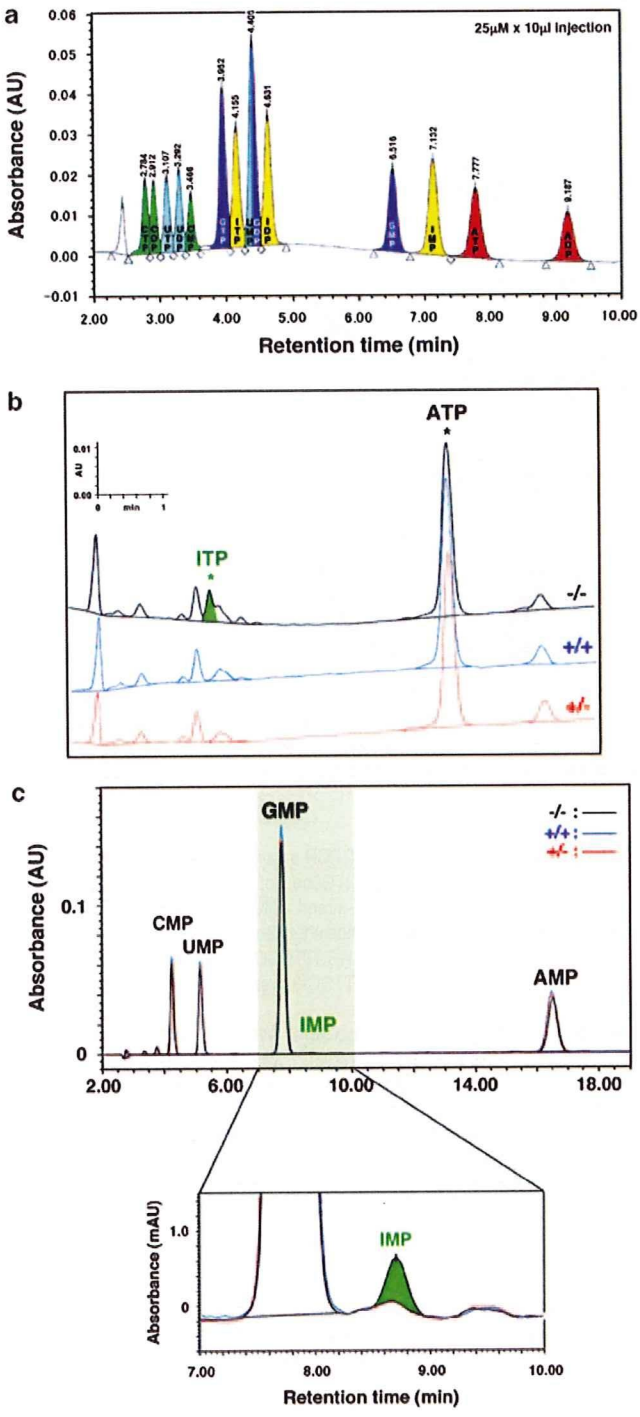

Figure 6 Accumulation of inosine nucleotide in the *Itpa*$^{-/-}$ mouse. The absorbance of each sample at 248.5 nm (the wavelength corresponding to the maximum absorbance of the inosine nucleotide at pH 6) was plotted. (**a**) HPLC conditions for the separation of nucleotides. A volume of 10 μl of a standard nucleotide mixture containing ATP, ADP, AMP, CTP, CDP, CMP, GTP, GDP, GMP, ITP, IDP, IMP, UTP, UDP and UMP (25 μM each) were chromatographed on a SunFire 5.0 μmC_{18} column (4.6 × 250 mm) as described in the Materials and Methods section. After each run, the column was washed with 50% methanol. Under these conditions, we obtained a good separation pattern except for UMP and GDP. The AMP peak was not included on the chart due to its long retention time (13.663 min). (**b**) Accumulation of ITP in the nucleotide pool of *Itpa*$^{-/-}$ mouse erythrocytes. The peak area corresponding to the accumulated ITP is shown in green. No ITP was evident in *Itpa*$^{+/+}$ and *Itpa*$^{+/-}$ mouse erythrocytes. (**c**) IMP detected in the total RNA of *Itpa*$^{-/-}$ mouse heart. To determine the amount of inosine nucleotide in RNA, we digested total RNA with the nuclease P1, a nd analyzed the digest on a C-18 column. The peak area of IMP observed in the *Itpa*$^{-/-}$ mouse is shown in green

Materials and Methods

Materials. Oligonucleotides were obtained from Genenet Co. Ltd. (Fukuoka, Japan). Recombinant Taq DNA polymerase and 1 Kb Plus DNA Ladder were obtained from Takara Bio Inc. (Otsu, Japan) and Invitrogen Japan K.K. (Tokyo, Japan), respectively. Anti-β-actin antibody (A-5316), ITP and other nucleotides were purchased from Sigma-Aldrich Japan K.K. (Tokyo, Japan). Nuclease P1 was obtained from Seikagaku Corporation (Tokyo, Japan).

Generation and analyses of the *Itpa*-gene disrupted mouse. To disrupt the *Itpa* gene, the λ-phage clones, λmITPA22 and λmITPA4,[23] which contain exons 1–6 and 2–7 of the mouse *Itpa* gene, respectively, were used to

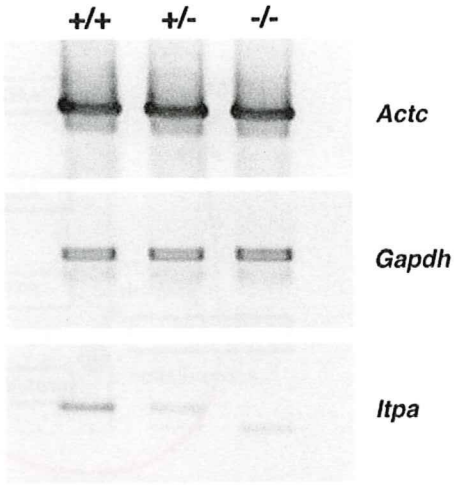

Figure 7 The expression of the *Actc* gene was not affected by *Itpa* gene disruption. The total RNA of each mouse heart was subjected to semiquantitative RT-PCR analysis. Amplification was performed for 25, 30 and 35 cycles. Results of the 25-cycle amplification are presented in the figure. The primer sequences used for RT-PCR were as follows: *Actc*, 5′-AATCCAGCCGCCCCTAGCACG-3′ and 5′-TGCAAGTCCTGGTCTGGTTTA-3′; *Gapdh*, 5′-CTGCCATTTGCAGTGGCAA AG-3′ and 5′-TGGTATTCAAGAGAGTAGGGA-3′; *Itpa*, 5′-AAGCTTGCCATGGCT GCGTCTTTGGTCG-3′ and 5′-AAGTCTTCTAGAATTTACATTTGC-3′

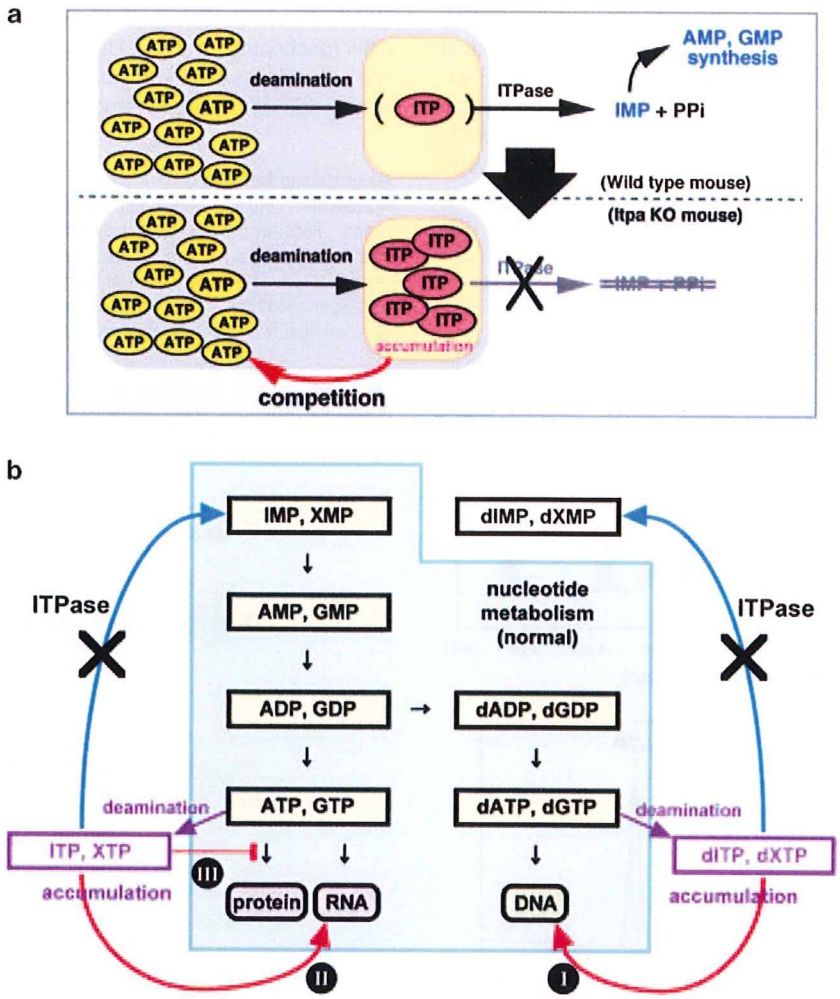

Figure 8 Quality control of the ATP pool in mouse by ITPase. (**a**) Sanitizing function of ITPase in the ATP pool. In the wild-type mouse, ITP, a deamination product of ATP, is hydrolyzed by ITPase to produce IMP, which is a normal intermediate metabolite of the purine biosynthesis pathway. ITP accumulates in cells when ITPase is absent. The accumulated ITP may act as a competitor of ATP in various kinds of bioreactions. (**b**) The function of ITPase in mouse cells. Quality control of the nucleotide pool is important not only because DNA (I) and RNA (II) are made up of the nucleotides which it supplies, but also because of the biological pathways that require nucleotides for activities (III), such as those involved in muscle contraction and heart development

construct a targeting vector. The targeting vector was constructed by replacing the 1.0 kbp *Xba*I–*Bam*HI region of a 9.5 kb genomic sequence, which contains exons 2–4, with the *polII*-neo cassette (Figure 1a). The targeting vector was then introduced into CCE ES cells by electroporation using standard procedures.[25] Two independently targeted ES clones were obtained and used to establish the knockout mouse strains. Disruption of the *Itpa* gene was confirmed by Southern blotting, PCR and RT-PCR. Southern blotting was performed using a ^{32}P-labeled *Eco*RI-*Nhe*I fragment as a 5′-flanking probe. The null expression of the ITPase protein in the *Itpa*$^{-/-}$ mouse was confirmed by western blotting using a rabbit anti-ITPase antiserum. ITPase activity was determined using erythrocyte extracts of the mice.

To determine the birth ratio of the *Itpa*$^{-/-}$ mouse, *Itpa*$^{+/-}$ mice (N1), which were the offspring of chimera male mice and C57BL/6J females, were used for mating. *Itpa*$^{-/-}$ mice were obtained by the mating of *Itpa*$^{+/-}$ mice (N1–N5). C57BL/6J mice were purchased from CLEA Japan Inc. (Tokyo, Japan). Echocardiograms were obtained using a Vevo660 imaging system (Vevo660, VisualSonics Inc., Toronto, Canada). All studies were approved by the Animal Care and Use Committee, Medical Institute of Bioregulation, Kyushu University.

PCR and RT-PCR. Tail DNA was used for the genomic PCR to determine the genotype of each mouse. The position and direction of each primer are shown in Figure 1a. The primer sequences used to determine the genotype were as follows: WT, 5′-CAGACAACCCTGAGTCACTAGGCTG-3′ and 5′-GTCTGTCTTCCTGTGT CCTGACTC-3′; KO, 5′-GTACATGTACATATCTATGTGGCCG-3′ and 5′-AGAGCG AGGGAAGCGTCTACCTA-3′. For RT-PCR analyses, total RNAs of liver and heart were prepared using ISOGEN (Nippon Gene Co. Ltd, Tokyo, Japan), according to the manufacturer's instructions. First-strand cDNA was synthesized with a First-Strand cDNA Synthesis kit (GE Healthcare Bio-Sciences K.K., Tokyo, Japan) using NotI-d(T)$_{18}$ primer. The primers 5′-AAGCTTGCCATGGCTGCGTCTTTGGTCG-3′ and 5′-AAGTCTTCTAGAATTTACATTTGC-3′ were used to amplify the *Itpa* cDNA.

Western blotting and antibodies. Western blotting analysis[26] and preparation of the anti-ITPase antiserum[23] were described earlier. The rabbit anti-ITPase antiserum (1/500 dilution), which was able to detect both human and mouse ITPase proteins with almost the same efficiency,[23] was used for the western blotting analysis. Proteins recognized by the anti-ITPase antiserum were detected by horseradish peroxidase-conjugated protein A with an ECL-Plus kit (GE Healthcare Bio-Sciences K.K.) using an LAS1000 Plus (Fuji Film Co., Tokyo, Japan) as a detector. The same membrane was treated with WB stripping solution (Nacalai Tesque Inc., Kyoto, Japan), and reused to detect β-actin by mouse monoclonal anti-β-actin antibody (A5316, Sigma-Aldrich Japan K.K.).

ITPase assay. ITPase activity was assayed by measuring the hydrolysis of ITP to IMP.[23] The red blood cells (RBCs) were washed three times with three volumes of 0.9% NaCl, and quickly frozen in LN_2. The frozen RBCs were lysed by adding a 10-fold volume of H_2O to obtain the erythrocyte extract. The protein concentration was determined with a Protein Assay system (Bio-Rad Laboratories Inc., Tokyo,

Japan) using bovine serum albumin (Thermo Fisher Scientific K.K., Yokohama, Japan) as a standard. The reaction mixture (50 μl) contained 50 mM Tris●HCl (pH 8.5), 50 mM $MgCl_2$, 1 mM DTT, 0.2 mM ITP and 2–20 μg of the erythrocyte extract to be examined. The reaction was run at 30°C for 15 min, and stopped by adding an equal volume (50 μl) of 10% trichloroacetic acid. The reaction mixture was neutralized with a 1/9 volume of 3 M K_2HPO_4, and applied to HPLC analysis.

Detection of inosine nucleotides by HPLC. Separation and quantification of nucleotides were performed by HPLC using a Waters Alliance 2690 separation module equipped with a Model 996 photodiode array detector (Nihon Waters K.K., Tokyo, Japan). A buffer consisting of 0.1 M K_2HPO_4 (pH 6.0) was used as the mobile phase without any organic solvent. To detect ITP in the nucleotide pool, an erythrocyte extract corresponding to 90 μg of protein was treated with 5% trichloroacetic acid, and the soluble fraction was analyzed by HPLC (SunFire 5.0 μmC_{18} column, 4.6 × 250 mm, Nihon Waters K.K.). To quantify the inosine nucleotide in the heart RNA, the total RNA (2.5 μg) was digested with 0.5 U of nuclease P1[27] at 50°C for 1 h, and separated on a Wakopak Handy ODS column (4.6 × 250 mm, Wako Pure Chemical Industries Ltd, Osaka, Japan).

Pathological analysis. Hematoxylin and eosin, and anti-desmin immunohistochemical staining were performed as described.[28] For the ultrastructural analysis, fixed heart sections were cut at a thickness of 70–80 nm, stained with 1% uranyl acetate followed by staining with a 1% lead citrate, 1% lead acetate and lead nitrate mixture, and were then examined with a JEM2000Ex (JEOL Ltd, Tokyo, Japan) electron microscope using an accelerating voltage of 80 KV.

Acknowledgements. We thank Dr. M Katsuki for CCE ES cells, Dr. Y Nakatsu for discussion, Y Yamada, M Sasaki, M Otsu, S Kitamura and A Matsuyama for technical assistance and Dr. W Campbell for comments on the manuscript. This study was supported by grants from Core Research for Evolutional Science and Technology (to YN), the Japan Science and Technology Agency, the Ministry of Education, Culture, Sports, Science, and Technology of Japan (18012035, 20012038 to KS), and the Japan Society for the Promotion of Science (19651097 to KS and 19390114 to DT).

1. Lindahl T. Instability and decay of the primary structure of DNA. *Nature* 1993; **362**: 709–715.
2. Mathews CK. DNA precursor metabolism and genomic stability. *FASEB J* 2006; **20**: 1300–1314.
3. Taddei F, Hayakawa H, Bouton M, Cirinesi A, Matic I, Sekiguchi M *et al* Counteraction by MutT protein of transcriptional errors caused by oxidative damage. *Science* 1997; **278**: 128–130.
4. Maki H, Sekiguchi M. Mut T protein specifically hydrolyses a potent mutagenic substrate for DNA synthesis. *Nature* 1992; **355**: 273–275.
5. Chung JH, Back JH, Park YI, Han YS. Biochemical characterization of a novel hypoxanthine/xanthine dNTP pyrophosphatase from *Methanococcus jannaschii*. *Nucleic Acids Res* 2001; **29**: 3099–3107.
6. Sakumi K, Tominaga Y, Furuichi M, Xu P, Tsuzuki T, Sekiguchi M *et al Ogg1* knockout-associated lung tumorigenesis and its suppression by *Mth1* gene disruption. *Cancer Res* 2003; **63**: 902–905.
7. Nakabeppu Y, Sakumi K, Sakamoto K, Tsuchimoto D, Tsuzuki T, Nakatsu Y. Mutagenesis and carcinogenesis caused by the oxidation of nucleic acids. *Biol Chem* 2006; **387**: 373–379.
8. Mo JY, Maki H, Sekiguchi M. Hydrolytic elimination of a mutagenic nucleotide oxodGTP by human 18-kilodalton protein: sanitization of nucleotide pool. *Proc Natl Acad Sci USA* 1992; **89**: 11021–11025.
9. Sakumi K, Furuichi M, Tsuzuki T, Kakuma T, Kawabata S, Maki H *et al.* Cloning and expression of cDNA for a human enzyme that hydrolyzes 8-oxo-dGTP a mutagenic substrate for DNA synthesis. *J Biol Chem* 1993; **268**: 23524–23530.
10. Rosenquist TA, Zharkov DO, Grollman AP. Cloning and characterization of a mammalian 8-oxoguanine DNA glycosylase. *Proc Natl Acad Sci USA* 1997; **94**: 7429–7434.
11. Radicella JP, Dherin C, Desmaze C, Fox MS, Boiteux S. Cloning and characterization of hOGG1 a human homolog of the OGG1 gene of *Saccharomyces cerevisiae*. *Proc Natl Acad Sci USA* 1997; **94**: 8010–8015.
12. Roldan-Arjona T, Wei YF, Carter KC, Klungland A, Anselmino C, Wang RP *et al.* Molecular cloning and functional expression of a human cDNA encoding the antimutator enzyme 8-hydroxyguanine-DNA glycosylase. *Proc Natl Acad Sci USA* 1997; **94**: 8016–8020.
13. Bjoras M, Luna L, Johnsen B, Hoff E, Haug T, Rognes T *et al* Opposite base-dependent reactions of a human base excision repair enzyme on DNA containing 7,8-dihydro-8-oxoguanine and abasic sites. *EMBO J* 1997; **16**: 6314–6322.
14. Lu R, Nash HM, Verdine GL. A mammalian DNA repair enzyme that excises oxidatively damaged guanines maps to a locus frequently lost in lung cancer. *Curr Biol* 1997; **7**: 397–407.
15. Aburatani H, Hippo Y, Ishida T, Takashima R, Matsuba C, Kodama T *et al.* Cloning and characterization of mammalian 8-hydroxyguanine-specific DNA glycosylase/apurinic, apyrimidinic lyase, a functional mutM homologue. *Cancer Res* 1997; **57**: 2151–2156.
16. Lin S, McLennan AG, Ying K, Wang Z, Gu S, Jin H *et al* Cloning, expression, and characterization of a human inosine triphosphate pyrophosphatase encoded by the *ITPA* gene. *J Biol Chem* 2001; **276**: 18695–18701.
17. Feng H, Dong L, Klutz AM, Aghaebrahim N, Cao W. Defining amino acid residues involved in DNA-protein interactions and revelation of 3′-exonuclease activity in endonuclease V. *Biochemistry* 2005; **44**: 11486–11495.
18. Dianov G, Lindahl T. Preferential recognition of I T base-pairs in the initiation of excision-repair by hypoxanthine-DNA glycosylase. *Nucleic Acids Res* 1991; **19**: 3829–3833.
19. Saparbaev M, Laval J. Excision of hypoxanthine from DNA containing dIMP residues by the *Escherichia coli*, yeast, rat, and human alkylpurine DNA glycosylases. *Proc Natl Acad Sci USA* 1994; **91**: 5873–5877.
20. Elder RH, Jansen JG, Weeks RJ, Willington MA, Deans B, Watson AJ *et al* Alkylpurine-DNA-N-glycosylase knockout mice show increased susceptibility to induction of mutations by methyl methanesulfonate. *Mol Cell Biol* 1998; **18**: 5828–5837.
21. Cardinal JW, Margison GP, Mynett KJ, Yates AP, Cameron DP, Elder RH. Increased susceptibility to streptozotocin-induced beta-cell apoptosis and delayed autoimmune diabetes in alkylpurine-DNA-*N*-glycosylase-deficient mice. *Mol Cell Biol* 2001; **21**: 5605–5613.
22. Chern CJ, MacDonald AB, Morris AJ. Purification and properties of a nucleoside triphosphate pyrophosphohydrolase from red cells of the rabbit. *J Biol Chem* 1969; **244**: 5489–5495.
23. Behmanesh M, Sakumi K, Tsuchimoto D, Torisu K, Ohnishi-Honda Y, Rancourt DE *et al* Characterization of the structure and expression of mouse Itpa gene and its related sequences in the mouse genome. *DNA Res* 2005; **12**: 39–51.
24. Hwang KY, Chung JH, Kim SH, Han YS, Cho Y. Structure-based identification of a novel NTPase from *Methanococcus jannaschii*. *Nat Struct Biol* 1999; **6**: 691–696.
25. Tsuzuki T, Sakumi K, Shiraishi A, Kawate H, Igarashi H, Iwakuma T *et al* Targeted disruption of the DNA repair methyltransferase gene renders mice hypersensitive to alkylating agent. *Carcinogenesis* 1996; **17**: 1215–1220.
26. Tsuchimoto D, Sakai Y, Sakumi K, Nishioka K, Sasaki M, Fujiwara T *et al* Human APE2 protein is mostly localized in the nuclei and to some extent in the mitochondria, while nuclear APE2 is partly associated with proliferating cell nuclear antigen. *Nucleic Acids Res* 2001; **29**: 2349–2360.
27. Fujimoto M, Kuninaka A, Yoshino H. Purification of a nuclease from *Penicillium citrinum*. *Agric Biol Chem* 1974; **38**: 777–783.
28. Dutta KK, Nishinaka Y, Masutani H, Akatsuka S, Aung TT, Shirase T *et al* Two distinct mechanisms for loss of thioredoxin-binding protein-2 in oxidative stress-induced renal carcinogenesis. *Lab Invest* 2005; **85**: 798–807.
29. Seidman JG, Seidman C. The genetic basis for cardiomyopathy: from mutation identification to mechanistic paradigms. *Cell* 2001; **104**: 557–567.
30. Towbin JA, Bowles NE. The failing heart. *Nature* 2002; **415**: 227–233.
31. Kumar A, Crawford K, Close L, Madison M, Lorenz J, Doetschman T *et al* Rescue of cardiac alpha-actin-deficient mice by enteric smooth muscle gamma-actin. *Proc Natl Acad Sci USA* 1997; **94**: 4406–4411.
32. Galperin MY, Moroz OV, Wilson KS, Murzin AG. House cleaning, a part of good housekeeping. *Mol Microbiol* 2006; **59**: 5–19.
33. Burton K, White H, Sleep J. Kinetics of muscle contraction and actomyosin NTP hydrolysis from rabbit using a series of metal-nucleotide substrates. *J Physiol* 2005; **563**: 689–711.
34. Kornberg A, Baker TA. The building blocks of DNA synthesis In: Kornberg A and Baker TA (eds) *DNA Replication* (2nd ed.) (WH Freeman and Company, NY, USA.) 2002 pp 53–54.
35. Sumi S, Marinaki AM, Arenas M, Fairbanks L, Shobowale-Bakre M, Rees DC *et al* Genetic basis of inosine triphosphate pyrophosphohydrolase deficiency. *Hum Genet* 2002; **111**: 360–367.
36. Maeda T, Sumi S, Ueta A, Ohkubo Y, Ito T, Marinaki AM *et al.* Genetic basis of inosine triphosphate pyrophosphohydrolase deficiency in the Japanese population. *Mol Genet Metab* 2005; **85**: 271–279.

Supplementary Information accompanies the paper on Cell Death and Differentiation website (http://www.nature.com/cdd)

Hydrogen in Drinking Water Reduces Dopaminergic Neuronal Loss in the 1-methyl-4-phenyl-1,2,3,6-tetrahydropyridine Mouse Model of Parkinson's Disease

Kyota Fujita[1], Toshihiro Seike[1], Noriko Yutsudo[2], Mizuki Ohno[2], Hidetaka Yamada[2], Hiroo Yamaguchi[2], Kunihiko Sakumi[2], Yukiko Yamakawa[1], Mizuho A. Kido[3], Atsushi Takaki[4], Toshihiko Katafuchi[4], Yoshinori Tanaka[5], Yusaku Nakabeppu[2☯], Mami Noda[1☯*]

1 Laboratory of Pathophysiology, Graduate School of Pharmaceutical Sciences, Kyushu University, Fukuoka, Japan, **2** Division of Neurofunctional Genomics, Medical Institute of Bioregulation, Kyushu University, Fukuoka, Japan, **3** Department of Oral Anatomy and Cell Biology, Graduate School of Dental Sciences, Kyushu University, Fukuoka, Japan, **4** Department of Integrative Physiology, Graduate School of Medical Sciences, Kyushu University, Fukuoka, Japan, **5** R&D Center, Home Appliances Manufacturing Business Unit, Panasonic Electric Works Co., Ltd., Osaka, Japan

Abstract

It has been shown that molecular hydrogen (H_2) acts as a therapeutic antioxidant and suppresses brain injury by buffering the effects of oxidative stress. Chronic oxidative stress causes neurodegenerative diseases such as Parkinson's disease (PD). Here, we show that drinking H_2-containing water significantly reduced the loss of dopaminergic neurons in PD model mice using both acute and chronic administration of 1-methyl-4-phenyl-1,2,3,6-tetrahydropyridine (MPTP). The concentration-dependency of H_2 showed that H_2 as low as 0.08 ppm had almost the same effect as saturated H_2 water (1.5 ppm). MPTP-induced accumulation of cellular 8-oxoguanine (8-oxoG), a marker of DNA damage, and 4-hydroxynonenal (4-HNE), a marker of lipid peroxidation were significantly decreased in the nigro-striatal dopaminergic pathway in mice drinking H_2-containing water, whereas production of superoxide ($O_2^{\bullet -}$) detected by intravascular injection of dihydroethidium (DHE) was not reduced significantly. Our results indicated that low concentration of H_2 in drinking water can reduce oxidative stress in the brain. Thus, drinking H_2-containing water may be useful in daily life to prevent or minimize the risk of life style-related oxidative stress and neurodegeneration.

Citation: Fujita K, Seike T, Yutsudo N, Ohno M, Yamada H, et al. (2009) Hydrogen in Drinking Water Reduces Dopaminergic Neuronal Loss in the 1-methyl-4-phenyl-1,2,3,6-tetrahydropyridine Mouse Model of Parkinson's Disease. PLoS ONE 4(9): e7247. doi:10.1371/journal.pone.0007247

Editor: David C. Rubinsztein, University of Cambridge, United Kingdom

Received September 2, 2008; **Accepted** September 2, 2009; **Published** September 30, 2009

Funding: Supported by Panasonic Electric Works Co., Ltd., and Kyushu University Global COE program for NY, MO, KS, YN. The funders had no role in study design, data collection and analysis, decision to publish, or preparation of the manuscript.

Competing Interests: The authors have declared that no competing interests exist.

* E-mail: noda@phar.kyushu-u.ac.jp

☯ These authors contributed equally to this work.

Introduction

It has been reported that molecular hydrogen (H_2) selectively reduces the hydroxyl radical, the most cytotoxic of the reactive oxygen species (ROS), and can thereby effectively protect cells. Thus, inhalation of H_2 gas strongly suppressed ischemic and reperfusion brain injury [1,2] and consumption of water saturated with H_2 (H_2 water) prevented stress-induced impairments in learning tasks during chronic physical restraint [3] by buffering the effects of oxidative stress or superoxide formation [4]. Oxidative stress, linked to mitochondrial damage, is also a primary cause of Parkinson's disease (PD) [5–7]. PD is regarded as an intractable neurodegenerative disease with pathological changes to dopaminergic neurons in the substantia nigra (SN) and nigro-striatal dopaminergic nerve terminals, leading to movement disorders such as tremor, rigidity and akinesia [8]. The 1-methyl-4-phenyl-1,2,3,6-tetrahydropyridine (MPTP)-based PD model has been important in elucidating the molecular cascade of cell death in dopaminergic neurons as well as the discovery of PD genes [9]. MPTP itself is not toxic, and as a lipophilic compound can cross the blood-brain barrier. Once inside the brain, MPTP is metabolized into the toxic cation 1-methyl-4-phenylpyridinium (MPP+) by the enzyme monoamine oxidase B (MAO-B) in glial cells. MPTP has a quite selective ability to cause neuronal death in dopaminergic cells, apparently through a high-affinity uptake process, through a dopamine transporter (DAT) [10], after it has been released from the glial cells. Inside dopaminergic neurons, MPP+ interferes with complex I of the electron transport chain, a component of mitochondrial metabolism, which leads to cell death and causes the buildup of free radicals, toxic molecules that contribute further to cell destruction [11].

Today, antioxidant compounds are widely recognized for the potential therapeutic treatment of oxidative stress diseases. Some antioxidant drugs and antioxidant materials in foods have been tested in the MPTP mouse model [12,13]. Antioxidants not only in foods but also in drinking water would offer a great advantage over other forms of antioxidant therapy. In fact, it was reported that drinking electrolyzed H_2-saturated water showed an effect in reduction of oxidative stress in rats, as measured by urine oxidized guanine and hepatic lipid peroxide [14]. Recently it was also shown that drinking H_2-saturated water, instead of inhaling H_2 gas, prevents cognitive impairment by reducing oxidative stress

[3]. According to Nagata et al. [3], even in drinking water, H_2 can be delivered to the blood in minutes.

Using the widely accepted PD model, we have tested the effect of H_2-containing drinking water on the MPTP-induced loss of dopaminergic neurons. Here we show that drinking H_2 water may potentially offer a great advantage over other forms of antioxidant therapy, particularly for chronic pathological conditions such as PD.

Results

Hydrogen water made by bubbling H_2 gas and using electrochemical reaction of magnesium

Hydrogen water (H_2 water) could be made by several methods. In the present experiments, H_2 water made by two relatively easy and safe ways was tested. The H_2 content in H_2 water, made by either dissolving electrolyzed hydrogen into pure water (H_2 bubbled water) or utilizing electrochemical reaction of magnesium with water (H_2/Mg water), declined with a half-time of ~2 h and almost disappeared after 8 h (Figure 1). The time course of H_2 content was similar in H_2 bubbled water and H_2/Mg water except at 4 and 6 h, suggesting that H_2 was better maintained in H_2/Mg water, though the mechanism was not clear.

The effect of H_2 water on acute MPTP neurotoxicity

To simply observe the effect of H_2 in drinking water, H_2-bubbled water was used for acute MPTP neurotoxicity tests. Mice were given H_2 water or non-H_2 water for 7 days prior to the MPTP administration and kept receiving it until the mice were killed and brains were extirpated. Since the H_2 content disappeared within 8 h (Figure 1), water supply was restricted to 8 h per day so that most of the water was taken by the mice during the first few hours of each day. Systemic administration of MPTP caused a significant decrease in the number of dopaminergic neurons in substantia nigra pars compacta (SNpc) (38% of that after saline & non-H_2 water) compared to those in saline injection group, as shown by the number of tyrosine hydroxylase (TH)-positive cells (Figure 2A). Dopaminergic fibers in the substantia nigra pars reticulosa (SNpr) were also apparently reduced. In mice treated with H_2 water, the loss of dopaminergic neurons in SNpc was about a half of that in mice drinking non-H_2 water (54% of saline & non-H_2 water) and showed a significant reduction in the loss of neurons in SNpc (Figure 2B). In saline injected groups, there were no apparent effects of H_2 on the number of dopaminergic neurons in SNpc (Figure 2A, 2B). This result was also supported by stereological analysis, a better method for unbiased cell counting (Figure 2C, 2D). The number of TH-positive neurons was significantly decreased by MPTP administra-

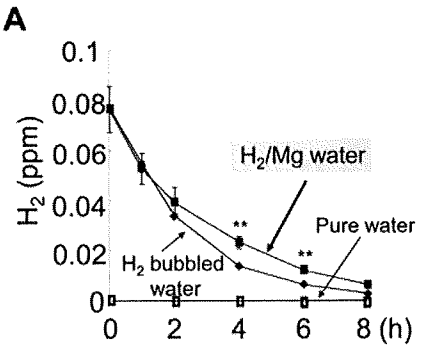

B

	pH
Pure water: H_2(-)	5.93
H_2 water (bubbled)	6.26
H_2 water (Mg)	8.76
$Mg(OH)_2$ water	8.52

Figure 1. Time-dependent decrease of H_2 content in each drinking water and their pH. Hydrogen water was made by directly bubbling H_2 gas produced by electrolysis (H_2 bubbled water) or chemical reaction using Mg (Mg/H_2 water). **$P<0.01$ compared to H_2 bubbled water. Error bars represent mean ± SEM.
doi:10.1371/journal.pone.0007247.g001

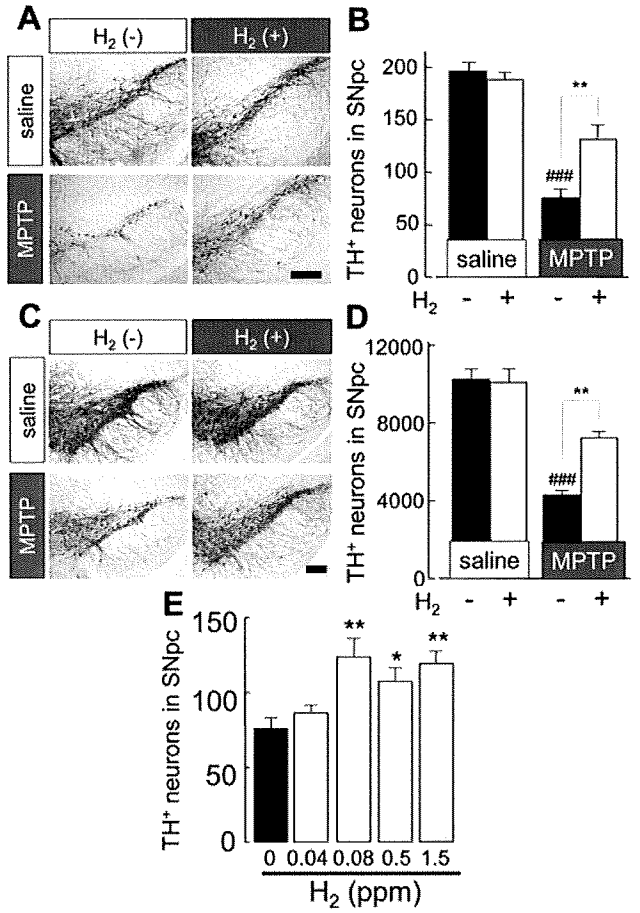

Figure 2. Drinking H_2 bubbled water reduced loss of dopaminergic neurons in substantia nigra induced by acute injection of MPTP. (A) Representative photomicrographs illustrating tyrosine hydroxylase (TH)-staining in substantia nigra (SN) of indicated treatment animal groups. TH-staining from mice with saline injection drinking non-H_2 water or H_2-bubbled water and those from MPTP-injected mice drinking non-H_2 water or H_2 bubbled water. Scale; 200 μm. (B) Average number of TH-positive neurons in SN pars compacta (SNpc), measured in 20 μm coronal sections (n = 4–6). (C) Representative photomicrographs illustrating TH immunoreactivity in the SN of indicated treatment animal groups. Staining is more intense than in (A) because of increased section thickness (30 μm) required for stereological analysis. Scale; 200 μm. (D) Quantification of TH-positive neurons by stereology, as described in Materials and Methods. (n = 4 each) (E) TH-positive neurons in SN from mice treated with 4 different concentration of H_2 (0.04, 0.08, 0.5, 1.5 ppm) in drinking water (n = 4–6). One-way ANOVA; ###$P<0.001$ compared to saline with non-H_2 water; *$P<0.05$, **$P<0.01$ compared to MPTP with non-H_2 water. Error bars represent mean ± SEM.
doi:10.1371/journal.pone.0007247.g002

tion, to 40% of controls (4180±309, MPTP & non-H_2 water; 10335±491, saline & non-H_2 water). However, drinking H_2 water significantly attenuated this decrease of neurons by MPTP without any decrease in saline injected mice (7105±325, MPTP & H_2 water; 10094±716, saline & H_2 water). Morphological observations also supported a lesser decrease of TH-immunoreactivity in both SNpc and SNpr. This rigorous stereological analysis fully supports the results obtained using conventional counting methods. Consequently, the protective effect of H_2 was proved by two different counting methods. The effects of H_2 water were dose-dependent, with a maximal effect at a much lower concentration (0.08 ppm) than saturated concentration of H_2 (1.5 ppm) (Figure 2E).

Mg/H_2 water and its effect on acute MPTP model mice

For further experiments, H_2/Mg water was used, which was made by a much easier and safer procedure. H_2/Mg water contained about 0.08 ppm H_2. H_2/Mg water showed a similar protective effect as H_2-bubbled water on the loss of dopaminergic neurons in acute MPTP model mice. Without MPTP administration, H_2/Mg water had no effect on the number of TH-positive cells (195±8; non-H_2/Mg water, 194±4; H_2/Mg water, Figure 3A, 3C).

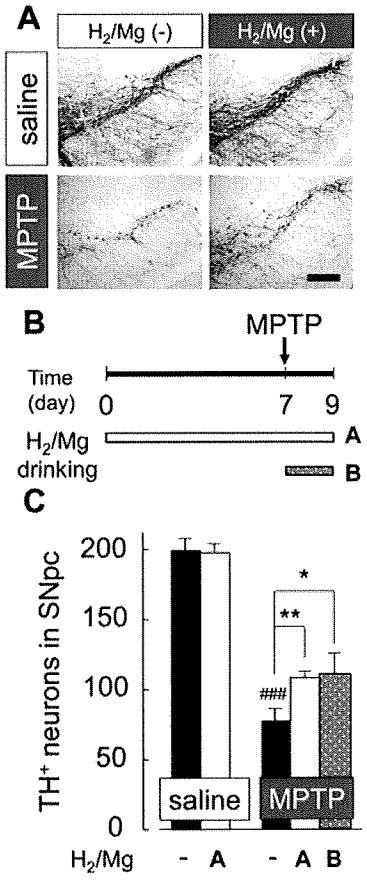

Figure 3. Drinking H_2/Mg water before and after acute injection of MPTP reduced loss of dopaminergic neurons. (A) TH-positive dopaminergic neurons in SN. Mice were treated with non-H_2 water or H_2/Mg water before and after acute MPTP injection. Scale; 200 μm. (B) Schedule for drinking H_2 water before (i) and after (ii) MPTP injection. (C) Average number of TH-positive neurons in mice with acute injection of saline or MPTP. One-way ANOVA; $^{###}P<0.001$ compared to saline with non-H_2 water; $^{*}P<0.05$, $^{**}P<0.01$ compared to MPTP with non-H_2 water. Error bars represent mean ± SEM.
doi:10.1371/journal.pone.0007247.g003

To test whether or not drinking H_2/Mg water was effective even after suffering oxidative stress, we compared two different procedures (Figure 3B); one was giving H_2/Mg water 7 days prior to the acute MPTP administration (Figure 3B; shown as i) and the other giving H_2/Mg water only after MPTP administration (Figure 3B; shown as ii). The result showed that drinking H_2/Mg water reduced the loss of dopaminergic neurons even after MPTP injection (Figure 3B, 3C; 16% & 17% recovery in drinking protocol shown as A&B, respectively). This may imply that drinking H_2 water might be effective even after the onset of oxidative stress-induced PD.

Since H_2/Mg water was alkaline (pH ~8.8, Figure 1), we tested the effect of alkalinized water (up to pH 8.8) made by adding $Mg(OH)_2$ to pure water. We also tested the effect of Mg and other metal elements, Al and Zn which might possibly exist in H_2/Mg water, by leaving the H_2/Mg water for 24 h (degassed H_2/Mg water) so that all the H_2 had gone. Neither of these solutions had any protective effect against MPTP-derived neurotoxicity (Figure 4A, 4B). Thus, the effect of the H_2/Mg water was not due to metal elements or to its alkalinity but to its content of H_2.

MPTP is converted into MPP+ which is indispensable for MPTP-derived neurotoxicity. We therefore measured the amount of MPP+ in the striatum where it was incorporated by DAT. The amount of MPP+ in the striatum was not significantly different in animals drinking H_2 water and non-H_2 water (Figure 4C). Therefore, the effect of H_2 water against the loss of dopaminergic

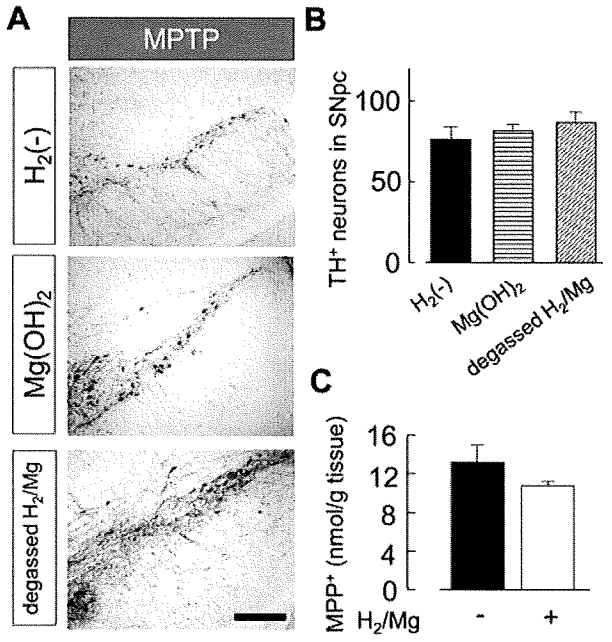

Figure 4. H_2, but not Mg ion and alkalinity, protected the neuronal damage from acute MPTP neurotoxicity. (A) TH-positive neurons in SN in mice drinking pure water (non-H_2 water), $Mg(OH)_2$ water or degassed H_2/Mg water. Neither $Mg(OH)_2$ water nor degassed H_2/Mg water had significant effect on MPTP neurotoxicity. (B) Average number of TH-positive neurons in SNpc in mice drinking non-H_2 water, $Mg(OH)_2$ water, and degassed H_2/Mg water. (C) The amount of MPP+ in striatum in mice drinking H_2/Mg water (white) and pure water (black) was not significantly different. MPP+ was measured 3 h after the last MPTP administration, when the concentration of MPTP reached maximum. One-way ANOVA. Error bars represent mean ± SEM.
doi:10.1371/journal.pone.0007247.g004

neurons in SNpc by MPTP was not related to the metabolism of MPTP.

The effect of H_2 water in chronic MPTP infusion model

Despite the lack of parkinsonian symptoms in the acute MPTP model in rodents, probably due to the low level of MAO-B in the rodent brain's capillaries [15], behavioral impairment could be observed in the chronic MPTP infusion model using an osmotic minipump to deliver the MPTP for long period [16]. This could provide a better model for human PD. In this experiment, mice were supplied with H_2 water or non-H_2 water 7 days prior to the pump implantation and the water supply continued until brain extirpation 28 days later (Figure 5A). Chronic infusion of MPTP induced a loss of TH-positive dopaminergic neuron in SNpc (Figure 5B). In mice drinking H_2 water, the loss of TH-positive cells (76% of control: saline & non-H_2 water) was less than that in mice drinking non-H_2 water (56% of control: saline & non-H_2 water) (Figure 5C). For the behavioral test, the ambulation scores in the open-field test were compared. Using the slightly modified open-field test reported previously [16], the ambulation score was expressed as percentage of that obtained in the first trial. Drinking H_2 water did not show any significant change in the ambulation score in mice with saline infusion (69±3% with non-H_2 water and 73±6% with H_2 water, respectively). The ambulation score in mice with chronic MPTP infusion with non-H_2 water was 40±4%, while in mice with H_2 water was 54±4% (Figure 5D). Other behavioral tests, for example the rotarod test and tail suspension test, were also examined but no significant effects were observed following chronic MPTP infusion (data not shown).

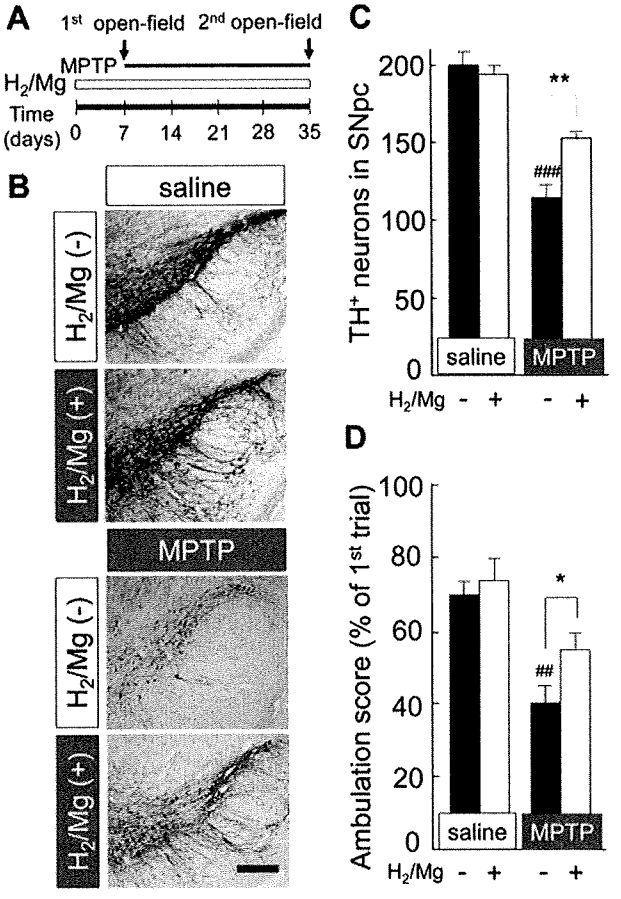

Figure 5. Drinking H_2/Mg water attenuated neurotoxicity and behavioral phenotype induced by chronic infusion of MPTP. (A) Schedule for continuous infusion of MPTP and behavioral observation. Mice started to drink non-H_2 water or H_2/Mg water 1 week before infusion of minipump. The 1st open-field test was performed in the morning of pump infusion. The 2nd test was performed 28 days after pump infusion. (B) TH-staining from mice with saline-infusion drinking non-H_2 water (I) or H_2/Mg water (II) and those from mice with MPTP-infusion drinking non-H_2 water (III) or H_2/Mg water (IV). (C) Average number of TH-positive neurons in mice with saline- or MPTP-infusion (n = 6). Brain samples were obtained from six 20 μm coronal SN sections. (D) Suppression of open-field activity by chronic infusion of MPTP was partially recovered by drinking H_2/Mg water. Relative ambulation score at the 2nd measurement was expressed as percentage of the 1st measurement (n = 6 for each group). One-way ANOVA; ###$P<0.001$ compared to saline with non-H_2 water; *$P<0.05$, **$P<0.01$ compared to MPTP with non-H_2 water. Error bars represent mean ± SEM.
doi:10.1371/journal.pone.0007247.g005

Hydrogen water reduced 4-HNE production in SN dopaminergic neuron

4-HNE is an aldehyde toxic end product of lipid peroxidation and one of the markers of membrane lipid peroxidation induced by cytotoxic radicals such as •OH [17]. Also, 4-HNE is reported to mediate the induction of neuronal apoptosis in the presence of oxidative stress [18]. In the acute MPTP model, protein level of 4-HNE in midbrain is increased [12,19]. In saline-injected mice, 4-HNE immunoreactive fluorescence in TH-positive neuron was minimal (Figure 6A, 6B). In contrast, in MPTP-treated mice, 4-HNE fluorescence was increased significantly 24 h after the last injection of MPTP.

In mice drinking hydrogen water, the baseline level of 4-HNE fluorescence was unchanged, but the striking increase in fluorescence following MPTP administration was virtually annulled, to a level that was not significantly above baseline (Figure 6B).

Hydrogen water failed to reduce the production of intracellular superoxide in SN dopaminergic neuron

Intracellular superoxide ($O_2^{\bullet -}$) was detected by administration of $O_2^{\bullet -}$ indicator, dihydroethidium (DHE) [20]. When DHE is oxidized by $O_2^{\bullet -}$, it binds to DNA and a bright red fluorescence is observed within the cell body.

The DHE intensity in TH-positive cell was significantly increased in the acute MPTP-treated mice compared to saline-treated mice (Figure 6A, 6B). Mice drinking hydrogen water appeared to show a slight decrease of DHE fluorescent intensity compared to non-hydrogen water mice with MPTP-injection, but this was not statistically significant ($p = 0.21$). As for microglia, which is one of the sources of superoxide release in SN, microglia did not show their activation 24 h, but 48 h after MPTP treatment. In mice drinking H_2 water, the morphological change of microglia was also observed 48 h, but not 24 h after MPTP administration (Figure S1).

Accumulation of cellular 8-oxoguanine in striatum

MPTP-induced loss of dopaminergic neuron is associated with the accumulation of 8-oxoguanine (8-oxoG) in the nigro-striatal pathway [5]. 8-oxoG is the major form of guanine oxidized by •OH, and is accumulated in both mitochondrial and nuclear DNA [21]. Hence, 8-oxoG is widely used as an index of DNA oxidative stress. The distinction between 8-oxoG accumulation in mitochondrial and nuclear DNA can be made using immunohistochemical techniques [5,22]. In our study, we investigated the accumulation of mitochondrial 8-oxoG in the striatum, where the dopaminergic nerve terminals end. Mitochondrial 8-oxoG showed significant accumulation in the striatum 24 h after acute MPTP administration.